NACA

RESEARCH MEMORANDUM

PERFORMANCE CHARACTERISTICS AT MACH NUMBERS TO 2.0 OF VARIOUS TYPES OF SIDE INLETS MOUNTED ON FUSELAGE OF PROPOSED SUPERSONIC AIRPLANE

IV - RECTANGULAR-COWL INLETS WITH TWO-DIMENSIONAL COMPRESSION RAMPS

By Paul C. Simon

Lewis Flight Propulsion Laboratory
Cleveland, Ohio

NATIONAL ADVISORY COMMITTEE FOR AERONAUTICS

WASHINGTON

October 28, 1952

1G

NATIONAL ADVISORY COMMITTEE FOR AERONAUTICS

RESEARCH MEMORANDUM

PERFORMANCE CHARACTERISTICS AT MACH NUMBERS TO 2.0 OF VARIOUS TYPES OF SIDE INLETS MOUNTED ON FUSELAGE OF PROPOSED SUPERSONIC AIRPLANE

IV - RECTANGULAR-COWL INLETS WITH TWO-DIMENSIONAL COMPRESSION RAMPS

By Paul C. Simon

2664

SUMMARY

An experimental investigation was conducted to determine the performance of side inlets having external compression ramps and rectangular cowls mounted on the fuselage forebody of a proposed supersonic airplane. Compression-ramp angles of 6° and 12°, simulating two positions of a variable-geometry inlet, were investigated at free-stream Mach numbers of 0, 0.63, and from 1.5 to 2.0 at angles of attack from 0° to 12°. The air-induction systems were investigated with and without inlet cowl side fairings. Ram scoops were installed beneath the inlet ramps for removal of the fuselage boundary layer.

The 12° ramp inlet without side fairings had a critical pressure recovery of 0.83 and a supersonic mass-flow spillage of 4 percent of theoretical maximum at its design free-stream Mach number of 2.0 and model cruise angle of attack of 3°. The installation of side fairings increased this critical recovery to 0.88 and reduced the spillage to zero. Side fairings had a negligible effect on the 6° ramp configuration at its design Mach number of 1.5.

Inlet flow characteristics remained independent of positive angles of attack up to 6°. The entrance of fuselage boundary-layer air into the inlet and flow separation about the windward cowl lip impaired the performance at the higher angles. This separation was aggravated by the addition of side fairings.

The rectangular inlet without fairings exhibited stable (no buzz) operation for the entire range of variables investigated. Addition of inlet side fairings to the 12° ramp inlet caused instability at angle of attack.

INTRODUCTION

Preliminary investigations have indicated that the diffusion efficiencies obtained for nose inlets can be approached by side or aft inlets operating in a uniform flow field provided that the fuselage boundary-layer air accumulated ahead of the inlet is prevented from entering the inlet (references 1 and 2). However, the flow field ahead of a side inlet may be greatly distorted by asymmetrical fuselage body shapes and cross-flow effects at angles of attack (references 3 and 4). A general investigation of side inlets installed on an asymmetrical body and incorporating boundary-layer scoops was conducted in the 8- by 6-foot supersonic tunnel of the NACA Lewis laboratory at Mach numbers of 0, 0.63, and from 1.5 to 2.0 at angles of attack from 0° to 12°. Previous reports in this series, the results of which are summarized in reference 5, have discussed the following types of side inlets: two-dimensional compression-ramp inlets with semicircular cowls (reference 6), inlets utilizing half of a conical spike (reference 7), and normal wedge inlets with semicircular cowls (reference 8). The present report discusses a rectangular-cowl inlet having two-dimensional compression ramps of 12° and 6° to similate two positions of a variable-geometry inlet. The inlets were investigated with and without sweptback inlet cowl side fairings.

2664

SYMBOLS

A	area
C_D	model external drag coefficient based on maximum fuselage cross-sectional area of 1.784 sq ft
M	Mach number
m	mass flow
P	total pressure
p	static pressure
Δp	average maximum pressure minus average minimum pressure
V	velocity
y	normal distance from inlet floor at plane of survey, in.
α	model angle of attack, deg
θ	external compression-ramp angle
ρ	density

Subscripts:

B	boundary-layer bleed system
c	canopy survey station, station 67.5
d	boundary-layer bleed duct
max	maximum
p	lip plus ramp projected area; mass flow based on projected area (0.0937 sq ft)
0	free stream
1	minimum inlet area station, model station 69.25
1'	inlet entrance pressure rake station, model station 70.75
2	diffuser exit pressure rake station, model station 97.25

Pertinent mass-flow ratios:

$\frac{m_2}{m_{0,p}} = \frac{m_2}{\rho_0 V_0 A_p}$	ratio of duct mass flow to mass flow in free-stream tube area equal to sum of inlet lip and compression ramp projected areas (0.0937 sq ft)
$\frac{m_2}{m_{0,1}} = \frac{m_2}{\rho_0 V_0 A_1}$	ratio of duct mass flow to mass flow in free-stream tube area equal to duct minimum area (approximately 0.083 sq ft)
$\frac{m_2}{m_{max}}$	ratio of duct mass flow to theoretical maximum mass flow (choking) occurring at duct minimum area
$\left(\frac{m_d}{m_0}\right)_B = \frac{m_d}{\rho_0 V_0 A_d}$	ratio of boundary-layer bleed duct mass flow to mass flow in free-stream tube area equal to duct area (0.0246 sq ft)

APPARATUS AND PROCEDURE

The twin-scoop side inlets were mounted symmetrically in the upper quadrants of the fuselage forebody of a one-fourth scale model of a proposed supersonic airplane as shown in figure 1(a). The pilot's canopy, which decelerates the flow ahead of the inlet, and typical fuselage cross sections are shown in figure 2.

The inlets consisted of rectangular-shaped cowls with two-dimensional, external compression ramps (fig. 1(b)). Details of the inlets are shown in figure 3. The 12° compression-ramp leading edge was longitudinally located to cause the resulting compression shock wave to stand slightly ahead of the cowl lip when the model was operated in a supersonic stream of Mach number 2.0. The ramp and cowl leading edges and inlet lip angle remained fixed when the ramp angle was reduced to 6°.

Each inlet was designed to incorporate side fairings which were swept back from the tip of the compression ramp to the inlet cowl (figs. 1(b) and 3).

The inlet axes were canted down 2° with respect to the fuselage axis to approximately aline the inlets with the anticipated local flow approach angle at the cruise angle of attack of 3° (fig. 3(d)).

The twin inlets had independent but geometrically similar internal subsonic diffuser ducts which discharged in an axial direction. The duct cross sections changed smoothly from a rectangular form at the entrance (model station 69.25) to a circular cross section at the exit (model station 97.25) (fig. 3(a)). Typical duct cross sections and the resulting area variations for both the 12° and 6° ramp angles are presented in figure 4.

Ram-type boundary-layer scoops were located beneath the inlet ramps for removal of the fuselage boundary-layer air. Internal boundary-layer ducts were situated aft of the scoops and made a constant area transition from a nearly rectangular cross section at the entrance to a circular cross section at the exit. The boundary-layer air in excess of that passing through the bleed ducts was spilled out of the open scoop sides (fig. 3). The bleed ducts discharged parallel to the main air-flow ducts at the exit station.

The boundary-layer scoop height was fixed at 0.8 inch to correspond to the experimentally determined canopy boundary-layer thickness for angle of attack α of 3° and free-stream Mach number M_0 of 1.5 to 2.0 (reference 6).

Instrumentation, testing technique, and data reduction methods are similar to those of reference 6. The mass flows through the inlets and the boundary-layer ducts were regulated by means of remotely controlled plugs attached to the model sting. A three component strain-gage balance which measured the internal duct forces, fuselage drags, and model base forces, but not the forces acting on the plugs, was used to determine the drag characteristics. The drag presented is the streamwise component of the measured balance force minus the internal thrust and base force. The thrust developed is the streamwise component of the change in momentum of the air passing through the inlets from the free stream to the diffuser exit. The momentum decrement associated with the flow in the boundary-layer ducts is included in the drag force.

Subcritical inlet instability or buzz was recorded by means of pressure-sensitive electronic pick-ups and recorders connected to static-pressure orifices located at the diffuser exit station.

The amplitude of the pressure fluctuations was expressed as the ratio $\Delta p_2/P_0$ where Δp_2 is the difference between the average maximum and average minimum pressures recorded at station 2. Only those pressure amplitudes of $\Delta p_2/P_0 \geq 0.05$ were assumed large enough to be associated with inlet instability.

The Reynolds number based on the length of the fuselage ahead of the inlets was approximately 29×10^6 in the supersonic Mach number range and 19×10^6 at Mach number 0.63.

RESULTS AND DISCUSSION

Supersonic Mach Number Range

Cruise angle of attack of 3°. - The inlet flow and model drag characteristics of the four inlet configurations tested are presented in figure 5 for various values of diffuser discharge Mach number M_2 at supersonic free-stream Mach numbers M_0 from 1.5 to 2.0 for the cruise angle of attack of 3°.

The experimentally determined canopy Mach numbers M_c existing immediately ahead of the inlet entrance are indicated in the figure key for the free-stream Mach numbers investigated. The values of $(m_d/m_0)_B$, defined as the ratio of the mass flow in the boundary-layer bleed duct to that in a free-stream tube having an area equal to the duct area, which are tabulated in figure 5 and elsewhere are those recorded during the variation of the main duct mass flow; their magnitude corresponds to approximately 10 percent of a typical turbojet required engine air flow. The bleed mass-flow ratio, when varied from 0.25 to 0.76, did not affect the main inlet performance at the cruise angle of attack and design Mach numbers. This indicates that the low-energy air rejected by the bleed duct did not enter the main duct, but was spilled externally out of the open scoop sides.

Total-pressure recovery is defined as the ratio of the total pressure measured at the diffuser exit station to the free-stream total pressure and includes subsonic diffuser losses. Total-pressure losses from the free-stream to the inlet ramp are considered negligible, based on the canopy flow survey of reference 6. The recoveries presented are therefore a true indication of the diffusion efficiency of the inlet when it is operating at the local canopy Mach number.

The turbojet engine-inlet matching line for typical engine B of reference 10 is also shown in figure 5.

The variation with diffuser discharge Mach number of the inlet mass-flow ratio, defined as the ratio of duct mass flow to the mass flow in a free-stream tube having an area equal to the sum of the lip and compression-ramp projected area, is presented in figure 5 for all configurations. The corresponding theoretical maximum mass-flow ratios based on canopy and free-stream Mach numbers are included to illustrate the magnitude of the main duct mass-flow spillage. For example, at Mach number 2.0 the 12° ramp inlet without side fairings (fig. 5(a)) captured approximately 96 percent of the theoretical maximum mass flow. The peak pressure recovery increased from 0.88 to 0.97 for the 12° ramp inlet when the flight Mach number was reduced from 2.0 to 1.5. The critical pressure recovery increased from 0.83 to 0.93 for a similar reduction in Mach number with a concomitant decrease in mass-flow ratio throughout the diffuser discharge Mach number range. The supercritical air flow spillage increased from 4 percent at M_0 of 2.0 to 15 percent at M_0 of 1.5.

Stable operation of the 12° ramp rectangular-cowl inlet was realized throughout the entire range of flight and diffuser discharge Mach numbers at 3° angle of attack, although the vortex sheet discussed in reference 9 moved from outside to inside the cowling as the entering flow was reduced. A lambda shock and flow separation are also present on the ramp. These phenomena are illustrated in the series of schlieren photographs of figure 6. This apparent contradiction of the vortex sheet buzz criterion may be due to the relatively low Mach number (M_c = 1.83) or to the slip line influencing only part of the periphery of the inlet.

Matching the 12° inlet configuration (fig. 5(a)) with the engine at M_0 of 2.0 will cause the inlet to operate well into the supercritical range at M_0 of 1.5. Accordingly, an inlet configuration designed to operate at M_0 of 1.5 was obtained by lowering the compression-ramp angle to 6°, thus simulating a variable-geometry inlet. The results are presented in figure 5(b).

Decreasing the compression angle to 6° reduced the pressure recovery at the higher Mach numbers but had no significant effect at M_0 of 1.5 and 1.7. The minimum drag, at the lower speeds, was reduced because of the decrease in air flow spillage (from approximately 15 percent to 5 percent at M_0 of 1.5). It should also be noted that the engine-inlet matching occurs near the critical inlet discharge Mach number for the 6° ramp at M_0 of 1.5.

Inlet side fairings (see fig. 3) were installed on the rectangular inlet to reduce the air spillage by preserving the two-dimensionality of the flow compressed by the inlet ramp. The performance of this modified rectangular-cowl inlet utilizing a 12° compression ramp is presented

in figure 5(c). The addition of inlet side fairings reduced the supercritical mass-flow spillage from 4 percent to essentially zero at M_0 of 2.0. Pressure recovery at critical flow increased from 0.83 to 0.88; however, peak pressure recovery was unchanged primarily because of the occurrence of inlet instability at the lowest discharge Mach number.

The performance of the 6° ramp inlet with side fairings is presented in figure 5(d). A comparison with figure 5(b) indicates that the fairings had a negligible effect on the aerodynamic characteristics of the main inlet, particularly at the lower free-stream Mach numbers. Also, the 6° ramp with side fairings exhibited acceptable inlet stability for the Mach number range investigated.

The combined theoretical oblique and normal shock pressure recovery for a 12° compression wedge at a Mach number of 1.83 is about 0.93 compared with an over-all recovery of 0.83 and 0.88 (critical) experimentally obtained for the rectangular cowl inlets operating without and with inlet side fairings, respectively. To determine whether these differences were due to supersonic or subsonic diffusion losses, the total-pressure losses were separated into two parts - total-pressure losses (1) from free-stream conditions to the inlet entrance rakes $\Delta P_{0-1'}$, and (2) from the inlet rakes to the diffuser exit $\Delta P_{1'-2}$ - and are presented for the various inlet configurations in figure 7. Since the entrance rakes were situated $1\frac{1}{2}$ inches aft of the cowl lip, the inlet losses $\Delta P_{0-1'}/P_0$ include the internal losses from the cowl lip (station 1) to the rake; however, these are believed to be comparatively small.

Figure 7(a) shows that at M_0 of 2.0 the measured inlet losses $\Delta P_{0-1'}/P_0$ are approximately twice the theoretical values for the inlet without side fairings, thus accounting for most of the difference in pressure recovery between theory and experiment. The losses from station 1' to 2 are quite low for all configurations, being of the order of 2 to 5 percent for critical diffuser Mach number. Analysis of these losses for a Mach number of 2.0 at the critical points for the two inlets indicates that the greater portion of the increase in recovery previously noted for the side fairing configuration occured in the subsonic diffuser.

To aid in explaining the differences between the calculated and measured losses from station 0 to 1', inlet entrance rake total-pressure profiles for the 12° ramp inlet are shown in figure 8(a) for a free-stream Mach number of 2.0 and a range of diffuser discharge Mach number.

The high energy core of the profiles is in general agreement with the theoretical shock losses (one oblique and one normal). The difference between the measured and theoretical values (shown in fig. 7) is probably

caused by boundary-layer accumulation on the compression-ramp surface after the fuselage boundary-layer air was removed. This is substantiated by the profiles of figure 8(a), which show a large reduction in stagnation pressure in the region adjacent to the inlet floor. A comparison of the entrance profiles for the configurations without and with inlet side fairings (figs. 8(a) and 8(b)) indicates that for those with side fairings the lower inlet losses were a result of a slight improvement in the high-energy core region.

The inlet profiles indicate that operation of the 12° ramp inlet at M_0 of 1.5 (fig. 8(c)) resulted in negligible pressure losses in the central area of the inlet, even though a detached shock occurred off the ramp, and that the inlet losses occurred on the ramp and the internal surface of the cowl lip. The increased inlet losses when the side fairings were added apparently were due to a decrease in the pressures of the central rake region (see figs. 8(c) and 8(d)).

As mentioned previously, lowering of the 12° ramp to 6° resulted in a reduction in pressure recovery at M_0 of 2.0 (figs. 5(a) and 5(b)). This reduction is partially explained by the inlet profiles shown in figure 8(e), which indicate that flow separation is occurring about the internal surface adjacent to the windward (rakes I and II) cowl lip of the inlet. These areas of separation increased as the inlet mass flow was reduced. The installation of side fairings had a negligible effect on the profile characteristics (figs. 8(e) and 8(f)).

The radial and circumferential distributions of total-pressure recovery at the diffuser exit are presented in figure 9 for the 12° and 6° inlets with and without side fairings. A core of high-energy air appears in the upper right-hand quadrant; low-energy air appears in the region of the duct that has undergone the greatest amount of turning and that initially had low-energy air at the entrance. The 6° ramp inlet with side fairing exhibited a region of flow separation (fig. 9(d)) despite the absence of separation at the entrance rake station. Addition of inlet side fairings had no appreciable effect on the pressure distribution. The difference in the maximum and minimum total pressures measured at the diffuser exit (compressor face) was 475 pounds per square foot, which amounts to a 16 percent deviation from the average pressure for the 12° ramp inlet with side fairings at M_0 of 2.0 (fig. 9(c)).

Angle of attack. - The variation of the inlet flow characteristics with diffuser discharge Mach number at angles of attack from 0° to 12° for all configurations at their design Mach numbers are presented in figure 10.

A large decrease in performance occurred from 9° to 12° angle of attack for all inlets and was associated with the effective decrease in the ratio of the bleed scoop height to the average boundary-layer thickness, as reported in reference 1. The addition of inlet side fairings

decreased the stable operating range for the 12° ramp inlet at moderate angles of attack (6° and 9°) and a free-stream Mach number of 2.0.

Entrance total-pressure profiles are presented in figure 11(a) for the 12° ramp inlet at a free-stream Mach number of 2.0 for angles of attack of 0°, 6°, 9°, and 12°. The profiles indicate that the flow adjacent to the inlet floor and the windward side of the entrance separated from the surface when the model was placed at angles of attack. Separation may be caused by the large inlet flow approach angle, which is estimated to be 6° or greater at the higher angles of attack. Profiles for the 12° ramp inlet with side fairings (fig. 11(b)) substantiate this conclusion because separation increased when the length of surface about which separation could occur was increased by the addition of side fairings. This breakdown of the flow apparently was entirely responsible for the drop-off in pressure recovery when the angle of attack was changed from 6° to 9°, since the canopy survey reported in reference 6 indicates no increases in the boundary-layer thickness ahead of the inlet for these angles. Entrance separation also contributed to the decrease in performance at 12° angle of attack.

Inlet rake profiles at angle of attack for the 6° ramp inlets are presented in figures 11(c) and 11(d) for a free-stream Mach number of 1.5. Flow separation was not observed for the conditions presented.

Diffuser exit total-pressure contours for the 12° ramp inlets operating at various angles of attack and a free-stream Mach number of 2.0 are presented in figure 12. The relative distribution of the pressures for the inlet without fairings (fig. 12(a)) was not appreciably altered by changes in angle of attack; however, at 6° and above, the concentration of high pressure rotated counterclockwise to a position coinciding with the vertical center line of the diffuser exit. Installation of the side fairings (fig. 12(b)) apparently reduced the rotation of the high-pressure region with angle of attack. The flow separation observed at the inlet entrance rake station apparently reattached to the diffuser duct surface before reaching the exit.

Subsonic Mach Number of 0.63

The values of total-pressure recovery and mass-flow ratio for the 6° ramp inlets are presented in figure 13 at a flight Mach number of 0.63 and angles of attack from 0° to 9°.

The mass-flow ratio $m_2/m_{0,1}$ is defined as the ratio of the duct mass flow to the mass flow in a free-stream tube area equal to the duct minimum area. Only the 6° ramp inlets were investigated because their minimum areas are larger than those of the 12° ramp inlets and thus more nearly satisfy the relatively large mass-flow requirements of a turbojet engine operating at subsonic Mach numbers.

At 3° angle of attack the supercritical experimental mass-flow ratio is 92 percent of the theoretical maximum mass flow calculated for choking at the geometric minimum area for either inlet. However, the inlet with side fairings has slightly better performance at angle of attack.

The matching diffuser discharge Mach numbers for engine B of reference 10 are indicated on the figure and show that for operation at both sea level and 35,000 feet large losses in inlet pressure recovery will be incurred. Assuming a variable-geometry inlet having a ramp angle of zero degrees results in the estimated data shown by the dashed line. A similar extrapolation was presented in reference 5 wherein a method of averaging local diffuser discharge Mach numbers from pressure rake data was used; however, in figure 13 the diffuser discharge Mach numbers were computed from mass flow and total pressure to satisfy one-dimensional continuity resulting in comparatively lower M_2 values. Reduction of the ramp angle to zero indicates that a pressure recovery of 0.90 can be obtained for engine B operating at 35,000 feet and M_0 of 0.63.

Static or Take-Off Conditions

Inlet performance at static or take-off conditions for the 6° ramp rectangular inlets with and without side fairings is presented in figure 14. The mass-flow ratio is based on maximum theoretical mass flow obtained from isentropic choking at the geometric minimum inlet area (station 1).

The inlet flow characteristics of both 6° ramp inlets were identical. Critical pressure recovery amounted to only 0.78, while the vena contracta effects reduced the mass-flow ratio by 25 percent. Inlet-engine matching for engine B indicated only 0.70 in recovery. Slight improvement in performance could be realized by reducing the ramp angle to zero as illustrated in the figure; however, if the loss of 40 percent of the ideal thrust for engine B (calculated by the method of reference 10) associated with the low pressure recoveries cannot be tolerated, then some additional technique for increasing the minimum inlet area, such as blow-in doors, would have to be incorporated.

SUMMARY OF RESULTS

The performance of rectangular-cowl side inlets mounted on the fuselage of a proposed supersonic airplane was investigated at static conditions and at Mach numbers of 0.63 and from 1.5 to 2.0 at angles of attack to 12°. The inlets utilized two-dimensional compression ramps and fuselage boundary-layer removal systems. The following results were obtained:

1. The addition of inlet side fairings to the 12° ramp, rectangular-cowl inlet reduced the supercritical mass-flow spillage from 4 percent to essentially zero and increased the critical pressure recovery from 0.83 to 0.88 at a free-stream Mach number of 2.0 and a model angle of attack of 3°. The fairings had a negligible effect on the aerodynamic characteristics of the 6° ramp inlet.

2. At a free-stream Mach number of 2.0 flow separation about the internal surface adjacent to the windward cowl lip of the inlet side was responsible for the decrease in performance of the 12° ramp inlets as the angle of attack was increased to 9°. The combined effect of inlet side separation and entering fuselage boundary layer resulted in a large decrease in performance at 12° angle of attack. This condition was aggravated by the addition of side fairings.

3. The rectangular inlet with either the 6° or 12° external compression ramps exhibited stable (no buzz) operation at the cruise angle of attack for the range of free-stream and diffuser discharge Mach numbers investigated. Inlet instability occurred at a free-stream Mach number of 2.0 for 6° and 9° angles of attack when inlet side fairings were installed on the 12° ramp inlet.

4. The inlet performance was independent of the operating conditions of the boundary-layer bleed duct system for all configurations tested at model angle of attack of 3°.

Lewis Flight Propulsion Laboratory
National Advisory Committee for Aeronautics
Cleveland, Ohio

REFERENCES

1. Goelzer, H. Fred, and Cortwright, Edgar M., Jr.: Investigation at Mach Number 1.88 of Half of a Conical-Spike Diffuser Mounted as a Side Inlet with Boundary-Layer Control. NACA RM E51G06, 1951.

2. Wittliff, Charles E., and Byrne, Robert W.: Preliminary Investigation of Supersonic Scoop Inlet Derived from a Conical-Spike Nose Inlet. NACA RM L51G11, 1951.

3. Allen, H. Julian, and Perkins, Edward W.: Characteristics of Flow over Inclined Bodies of Revolution. NACA RM A50L07, 1951.

4. Luidens, Roger W., and Simon, Paul C.: Aerodynamic Characteristics of NACA RM-10 Missile in 8- by 6-Foot Supersonic Wind Tunnel at Mach Numbers from 1.49 to 1.98. I - Presentation and Analysis of Pressure Measurements (Stabilizing Fins Removed). NACA RM E50D10, 1950.

5. Weinstein, M. I.: Performance of Supersonic Scoop Inlets. NACA RM E52A22, 1952.

6. Valerino, Alfred S.: Performance Characteristics at Mach Numbers to 2.0 of Various Types of Side Inlets Mounted on Fuselage of Proposed Supersonic Airplane. I - Two-Dimensional Compression-Ramp Inlets with Semicircular Cowls. NACA RM E52E02, 1952.

7. Allen, J. L., and Simon, P. C.: Performance Characteristics at Mach Numbers to 2.0 of Various Types of Side Inlets Mounted on Fuselage of Proposed Supersonic Airplane. II - Inlets Utilizing Half of a Conical Spike. NACA RM E52G08, 1952

8. Esenwein, Fred T.: Performance Characteristics at Mach Numbers to 2.0 of Various Types of Side Inlets Mounted on Fuselage of Proposed Supersonic Airplane. III - Normal-Wedge Inlets with Semicircular Cowl. NACA RM E52H20, 1952

9. Ferri, Antonio, and Nucci, Louis M.: The Origin of Aerodynamic Instability of Supersonic Inlets at Subcritical Conditions. NACA RM L50K30, 1951.

10. Schueller, Carl F., and Esenwein, Fred T.: Analytical and Experimental Investigation of Inlet-Engine Matching for Turbojet-Powered Aircraft at Mach Numbers up to 2.0. NACA RM E51K20, 1952.

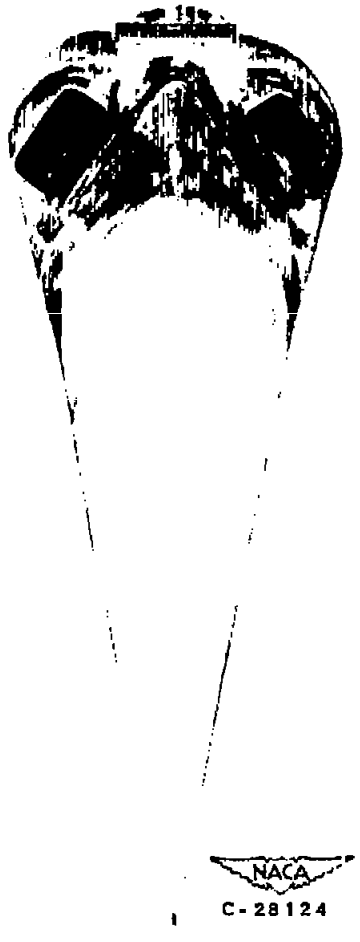

(a) Front view of model without fairings.

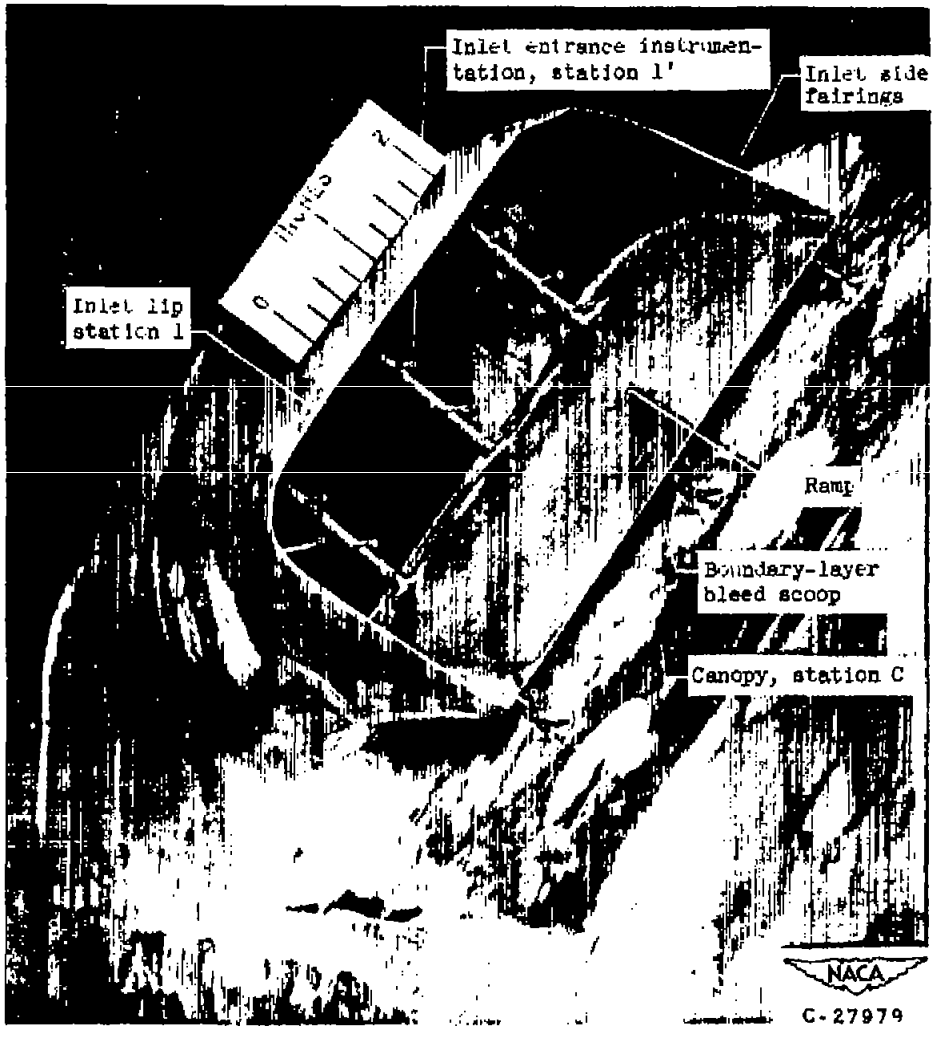

(b) Enlarged view of starboard inlet showing entrance instrumentation and inlet side fairings.

Figure 1. - Photographs of model.

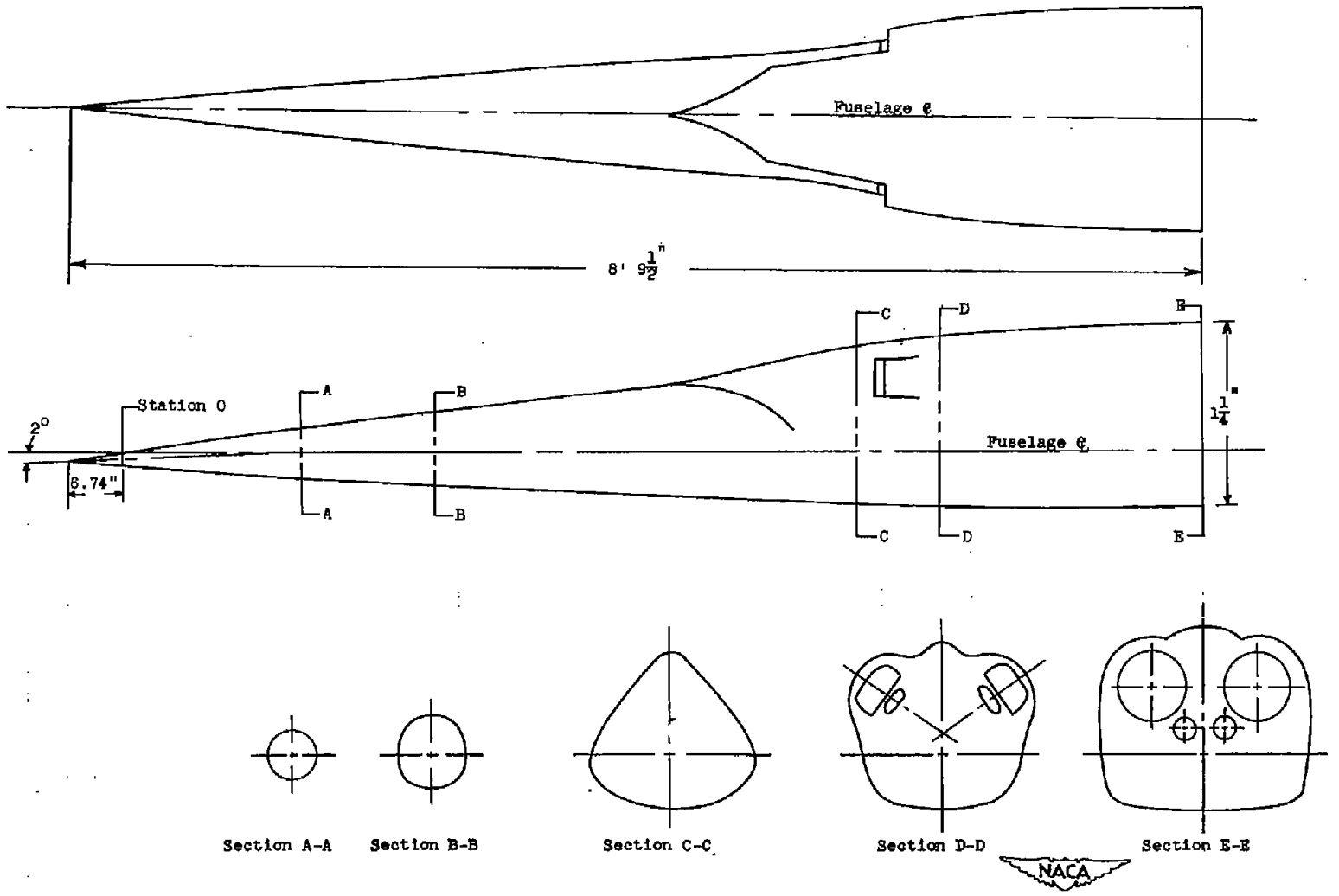

Figure 2. - Schematic diagram of model with representative cross sections.

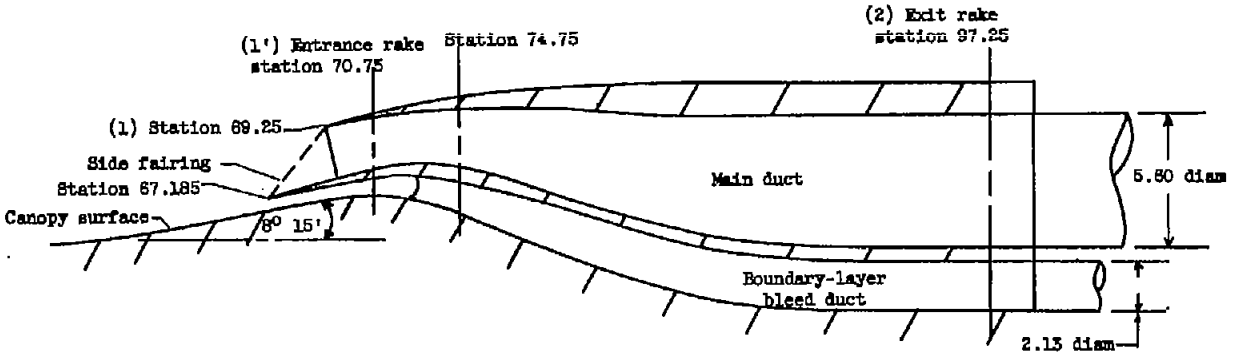

(a) Cross-sectional view of inlet.

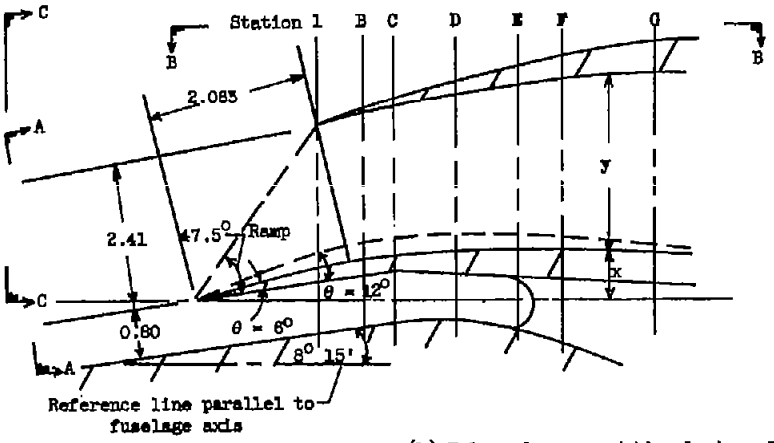

Station	Model station	6° Ramp		12° Ramp	
		x	y	x	y
1	69.25	0.52	2.20	0.76	1.96
B	70.00	0.68	2.23	0.83	1.97
C	70.80	0.71	2.28	0.97	2.02
D	71.50	0.77	2.40	1.01	2.165
E	72.50	0.78	2.55	1.00	2.33
F	73.25	0.77	2.66	0.97	2.46
G	74.75	0.75	2.83	0.87	2.72

(b) Enlarged cross-sectional view of inlet.

Figure 3. - Detailed views of rectangular-cowl inlet (all dimensions in inches).

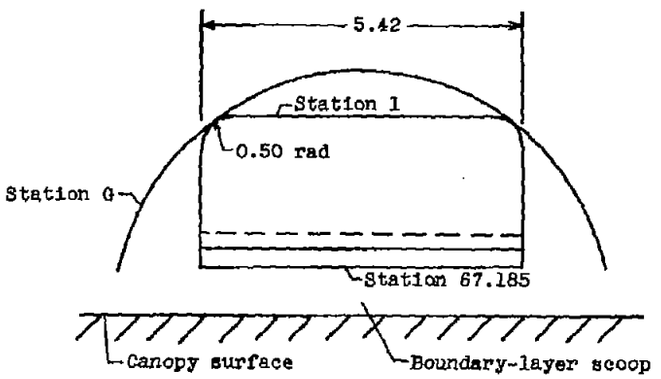

(c) View A-A.

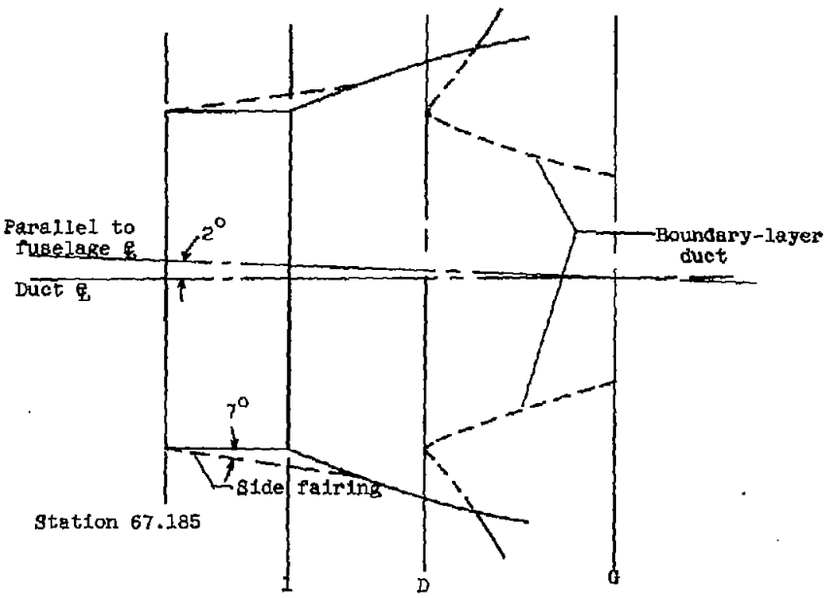

(d) View B-B.

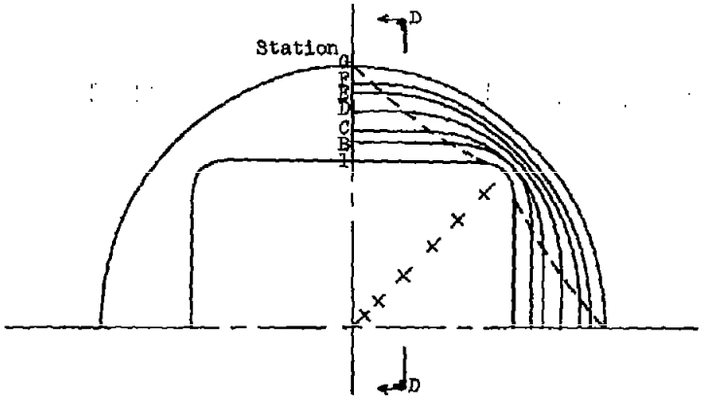

(e) View C-C.

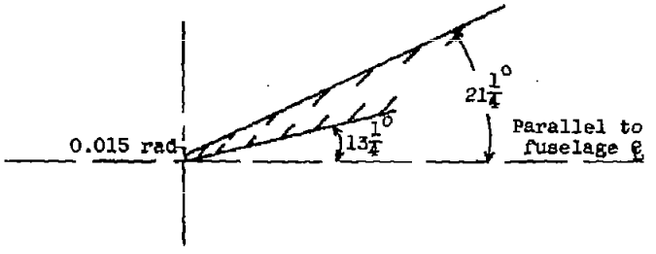

(f) Enlarged view of cowl lip section D-D.

NACA

Figure 3. - Concluded. Detailed views of rectangular-cowl inlet (all dimensions in inches).

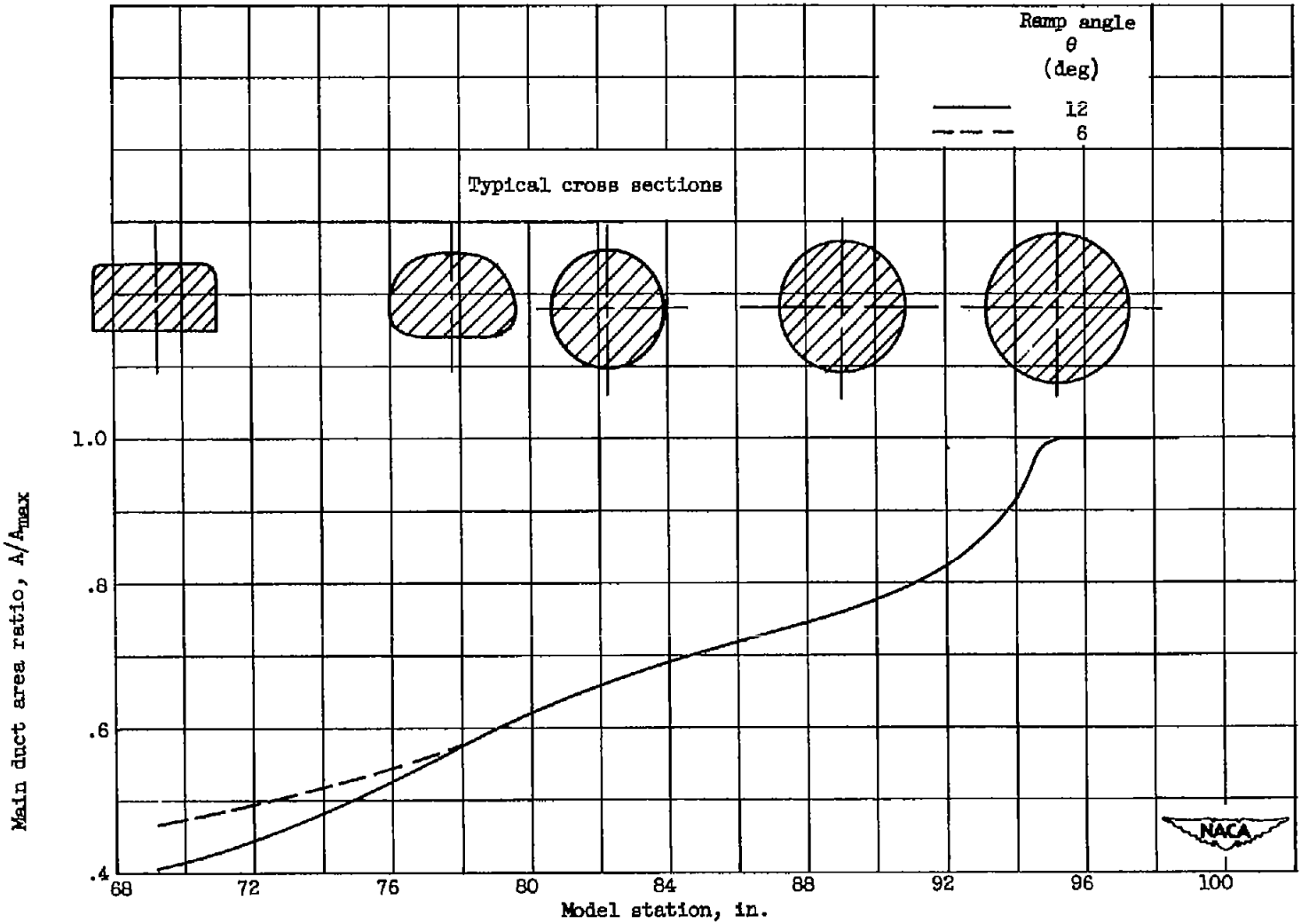

Figure 4. - Variation of main duct area ratio with model station for 12° and 6° ramp angles. Maximum main duct area is 0.1708 square foot.

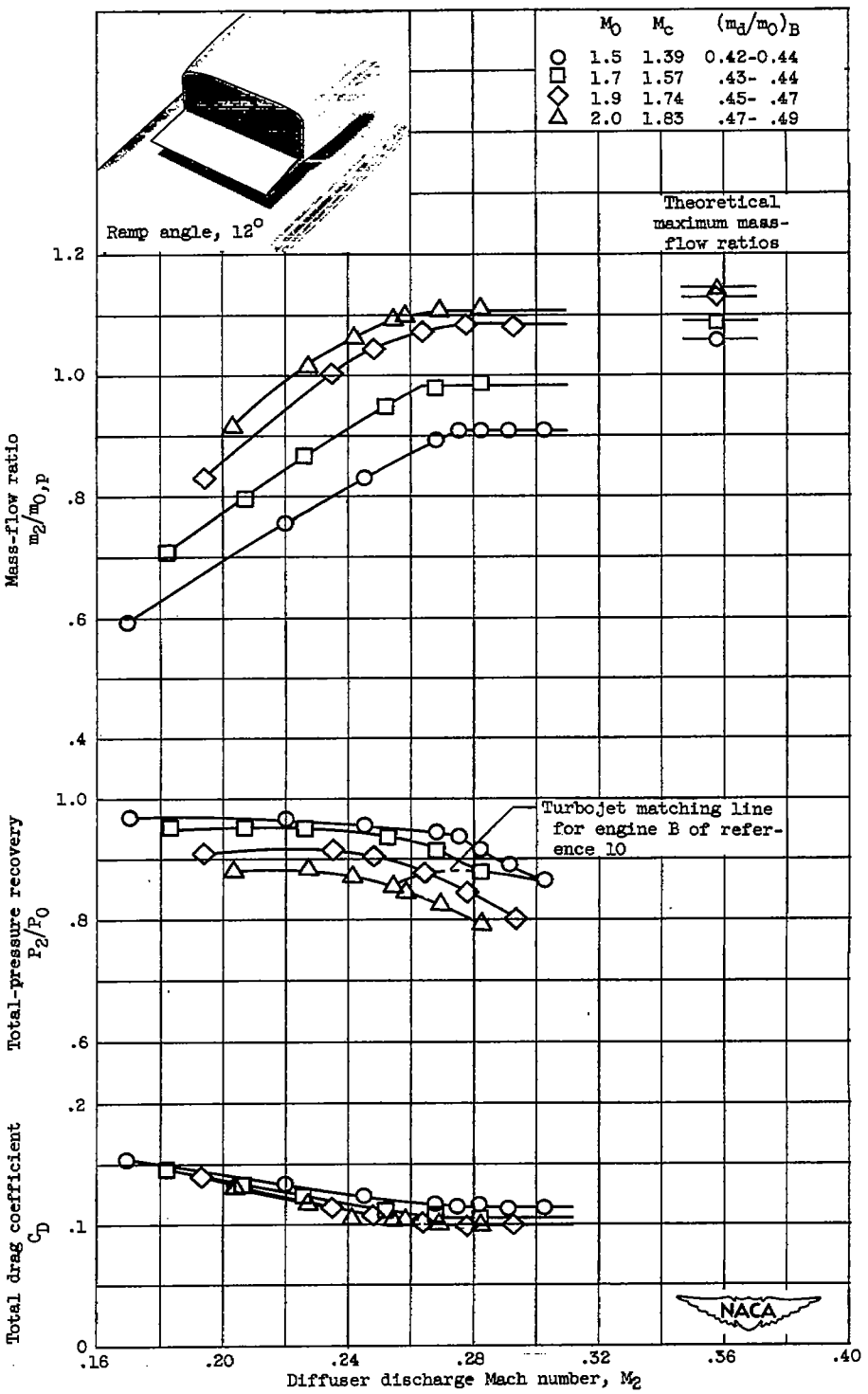

(a) Ramp angle, 12°.

Figure 5. - Variation of inlet characteristics with diffuser discharge Mach number for various supersonic flight Mach numbers at cruise angle of attack of 3°.

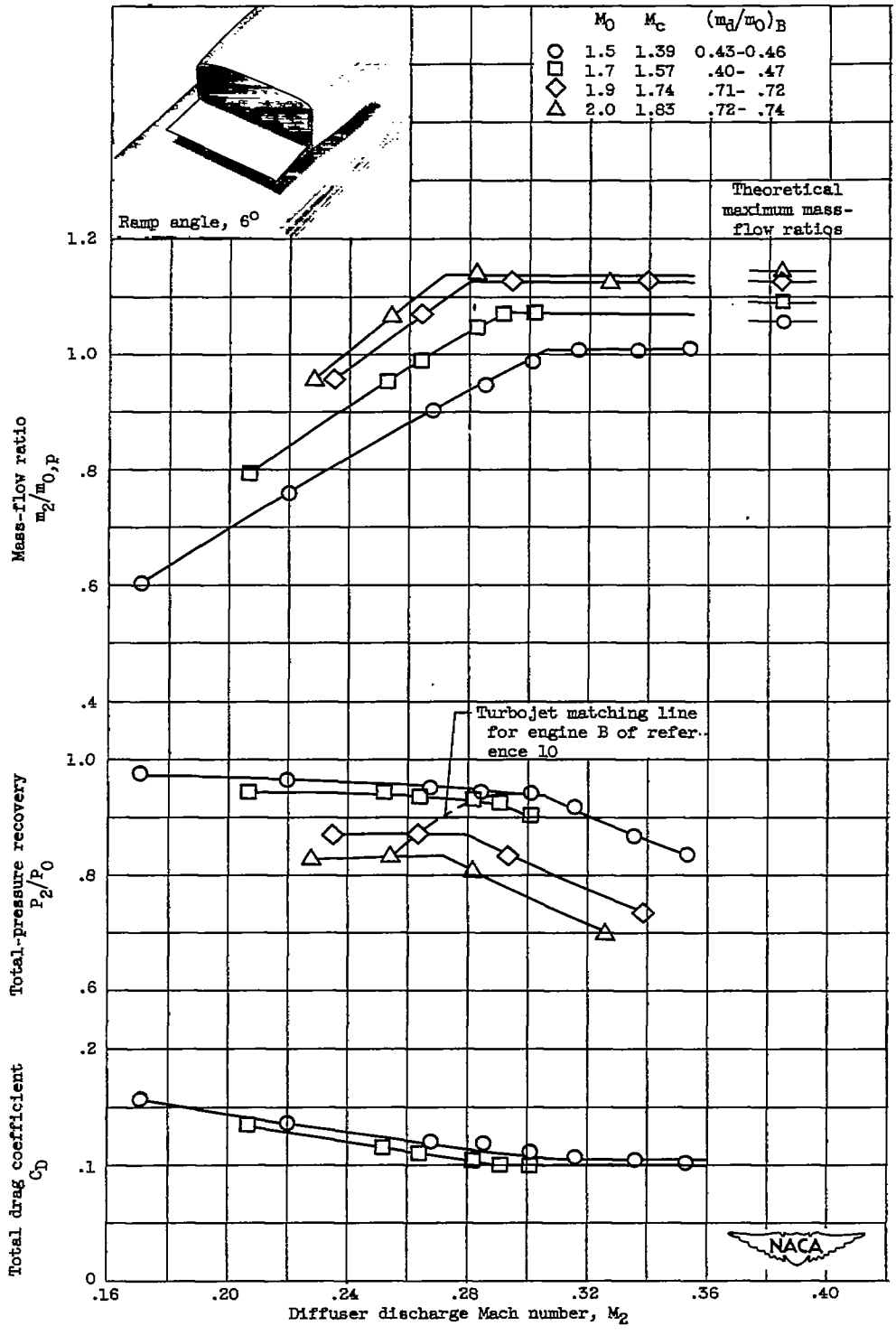

(b) Ramp angle, 6°.

Figure 5. - Continued. Variation of inlet characteristics with diffuser discharge Mach number for various supersonic flight Mach numbers at cruise angle of attack of 3°.

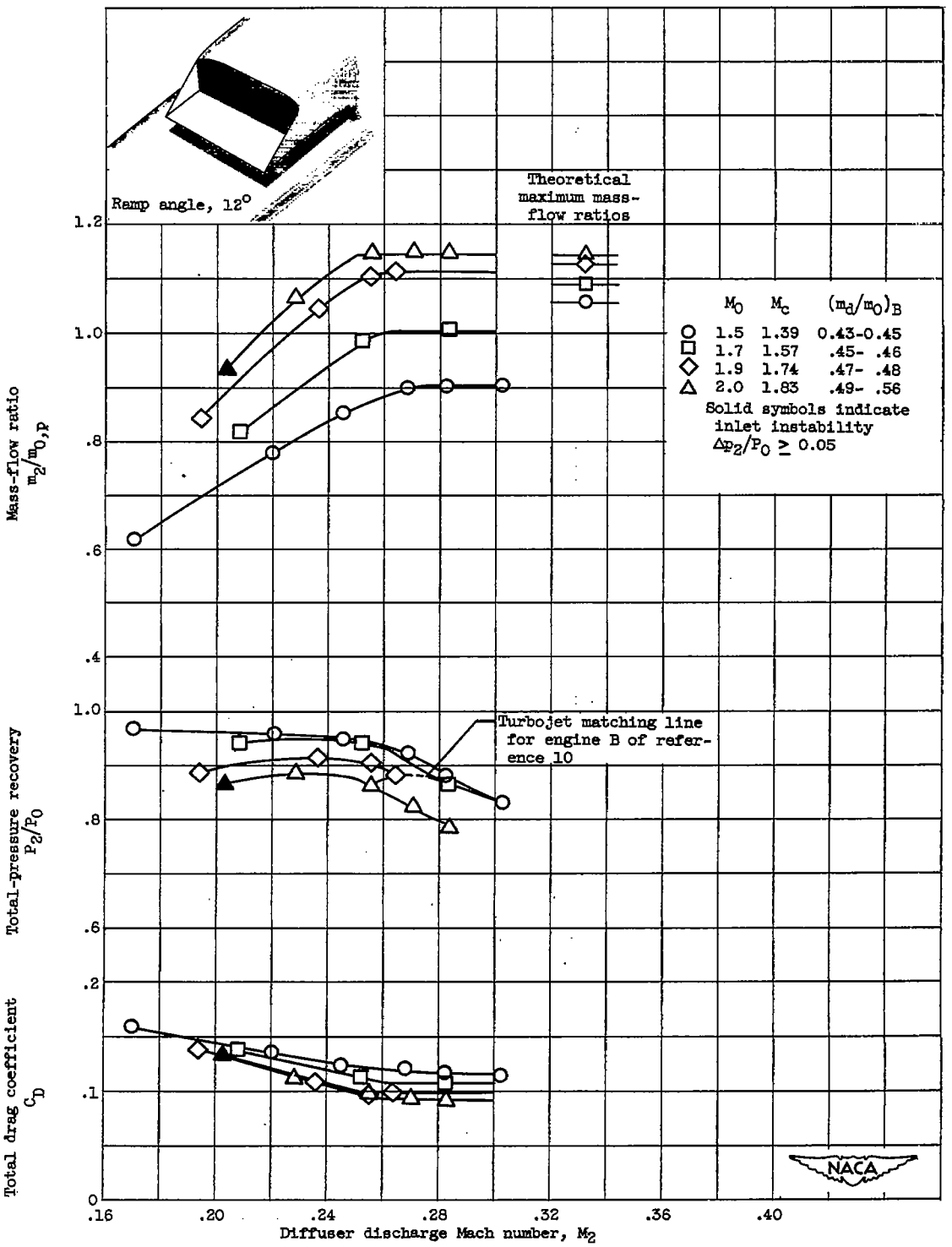

(c) Ramp angle, 12°; side fairings.

Figure 5. - Continued. Variation of inlet characteristics with diffuser discharge Mach number for various supersonic flight Mach numbers at cruise angle of attack of 3°.

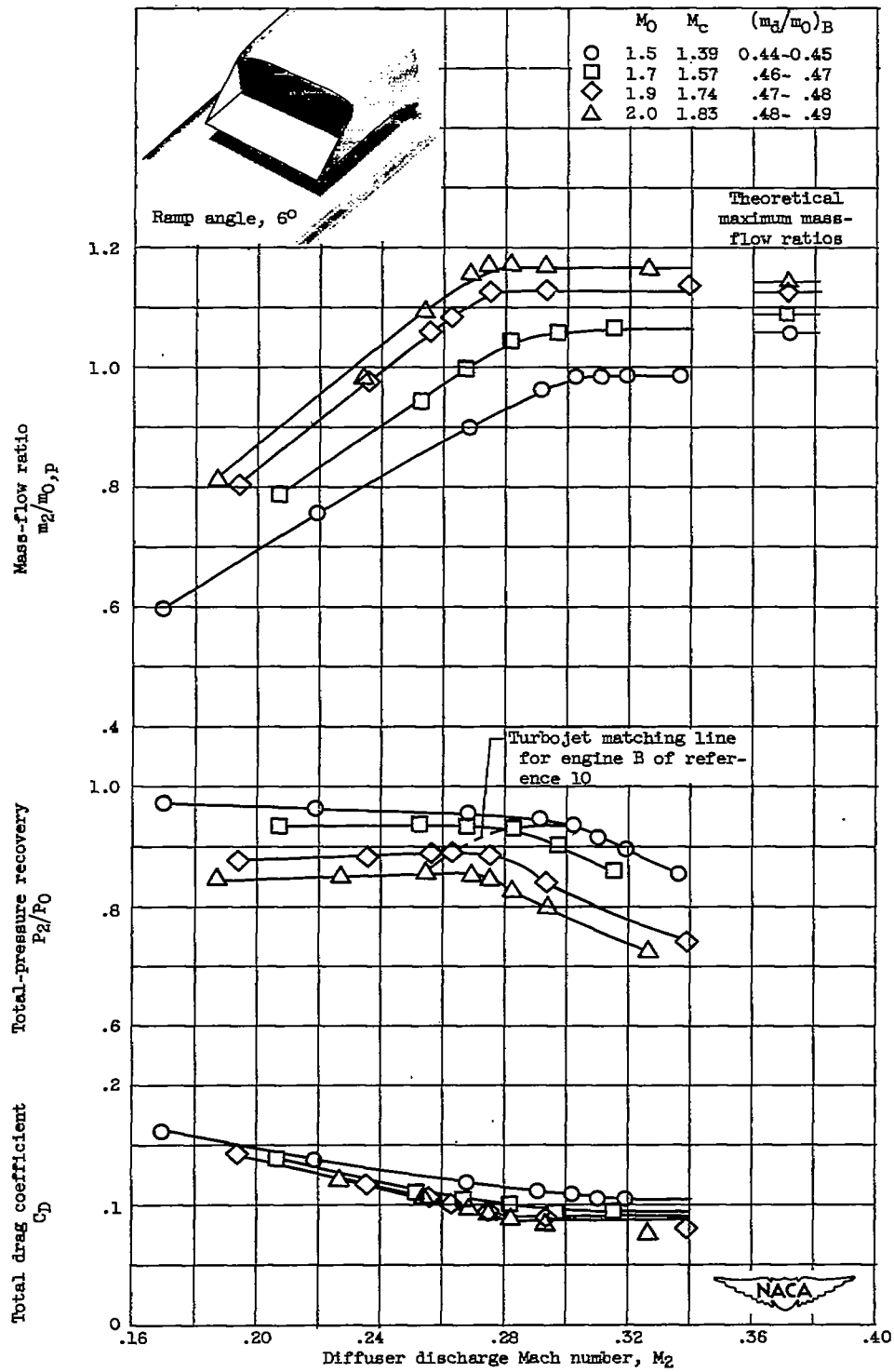

(d) Ramp angle, 6°; side fairings.

Figure 5. - Concluded. Variation of inlet characteristics with diffuser discharge Mach number for various supersonic flight Mach numbers at cruise angle of attack of 3°.

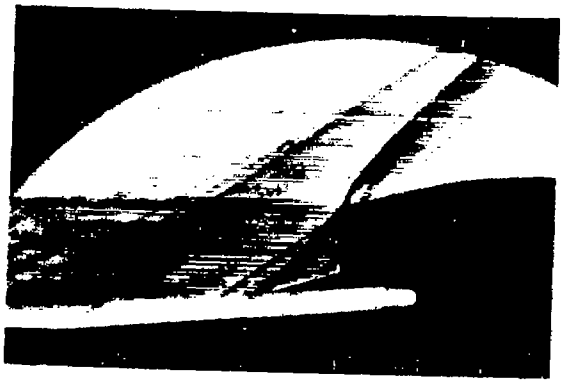

(a) Diffuser discharge Mach number, 0.282.

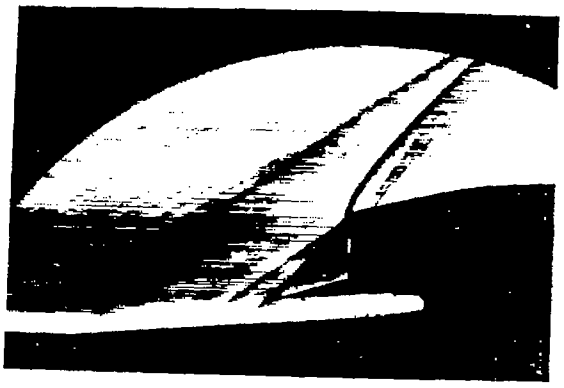

(b) Diffuser discharge Mach number, 0.255.

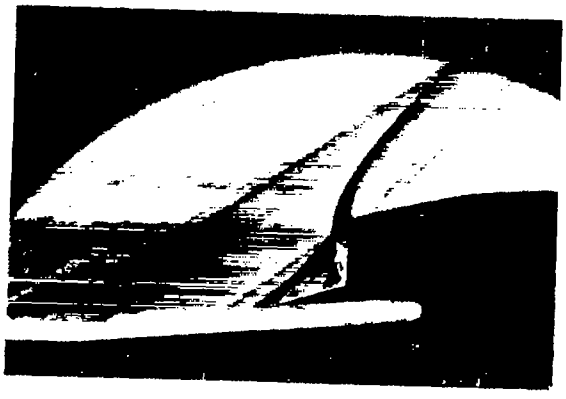

(c) Diffuser discharge Mach number, 0.241.

(d) Diffuser discharge Mach number, 0.228.

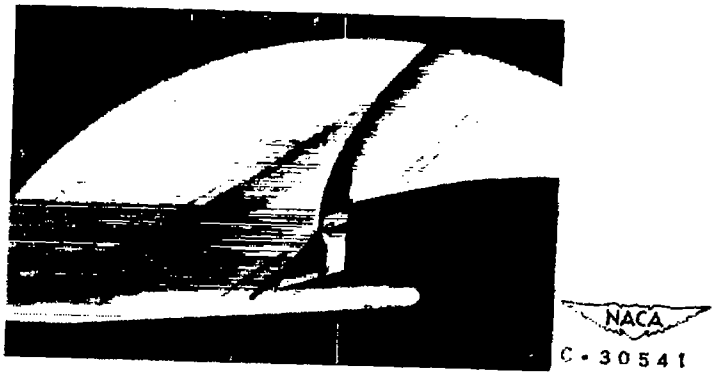

(e) Diffuser discharge Mach number, 0.203.

Figure 6. - Schlieren photographs of rectangular-cowl inlet with 12° external compression-ramp angle for various values of diffuser discharge Mach number. Free-stream Mach number, 2.0 (canopy Mach number, 1.83); angle of attack, 3°.

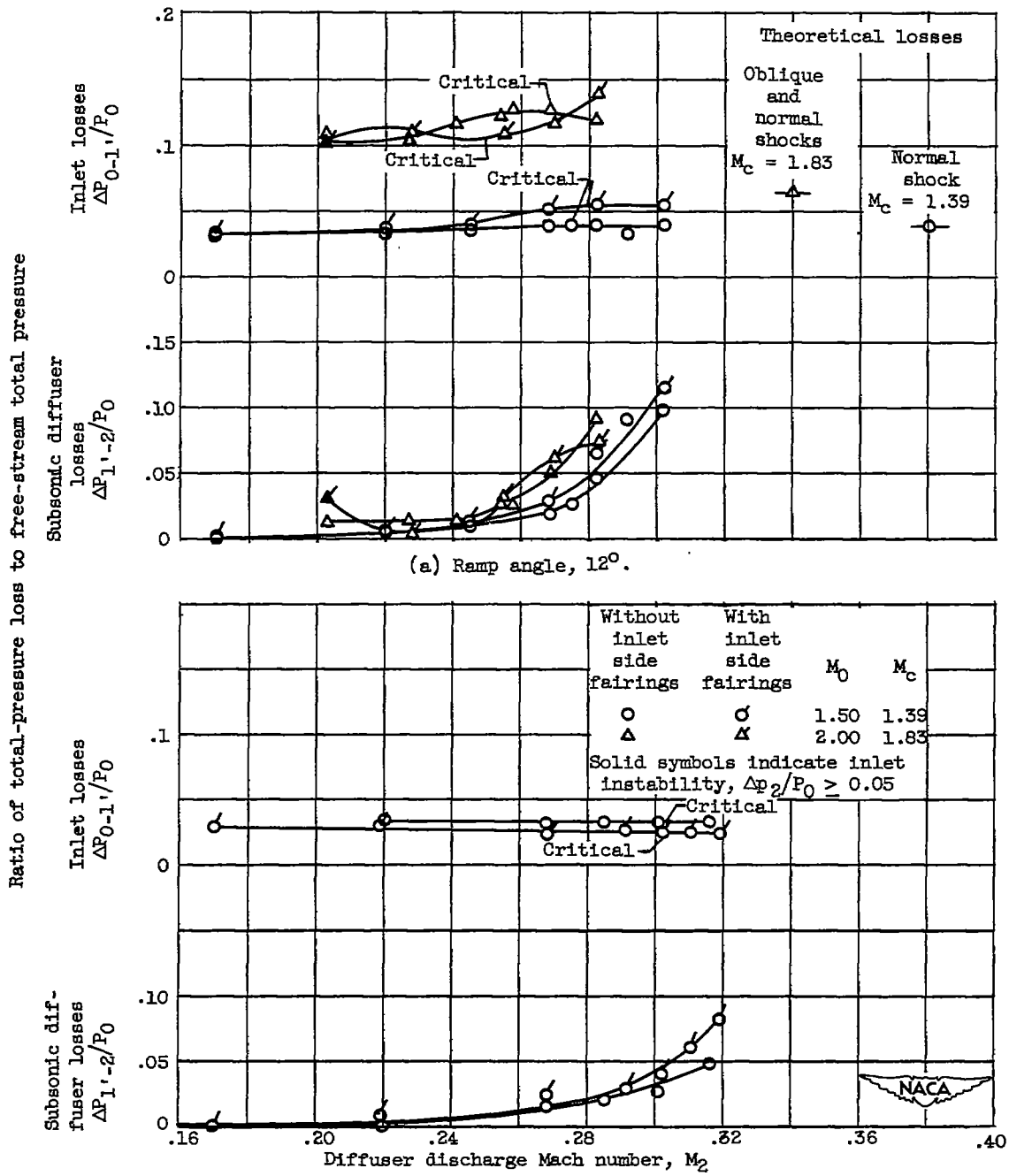

Figure 7. - Variation of total-pressure losses with diffuser discharge Mach number for inlets with 12° and 6° ramp angles with and without inlet side fairings at flight Mach numbers of 1.5 and 2.0 and angle of attack of 3°.

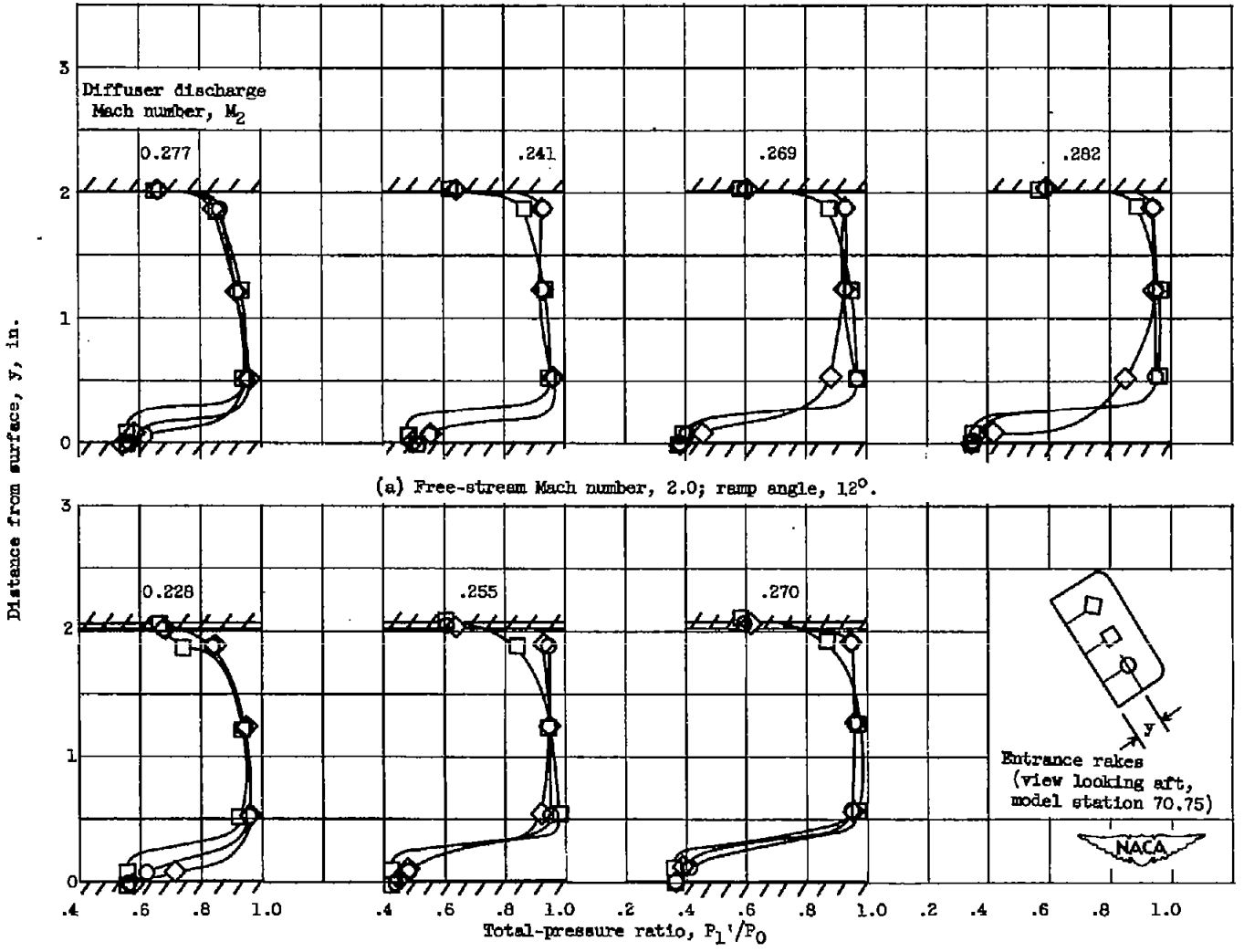

(a) Free-stream Mach number, 2.0; ramp angle, 12°.

(b) Free-stream Mach number, 2.0; ramp angle, 12°; side fairings.

Figure 8. - Inlet entrance total-pressure ratio profiles for inlets with 12° and 6° ramp angles with and without inlet side fairings at free-stream Mach numbers of 1.5 and 2.0 and angle of attack of 3°.

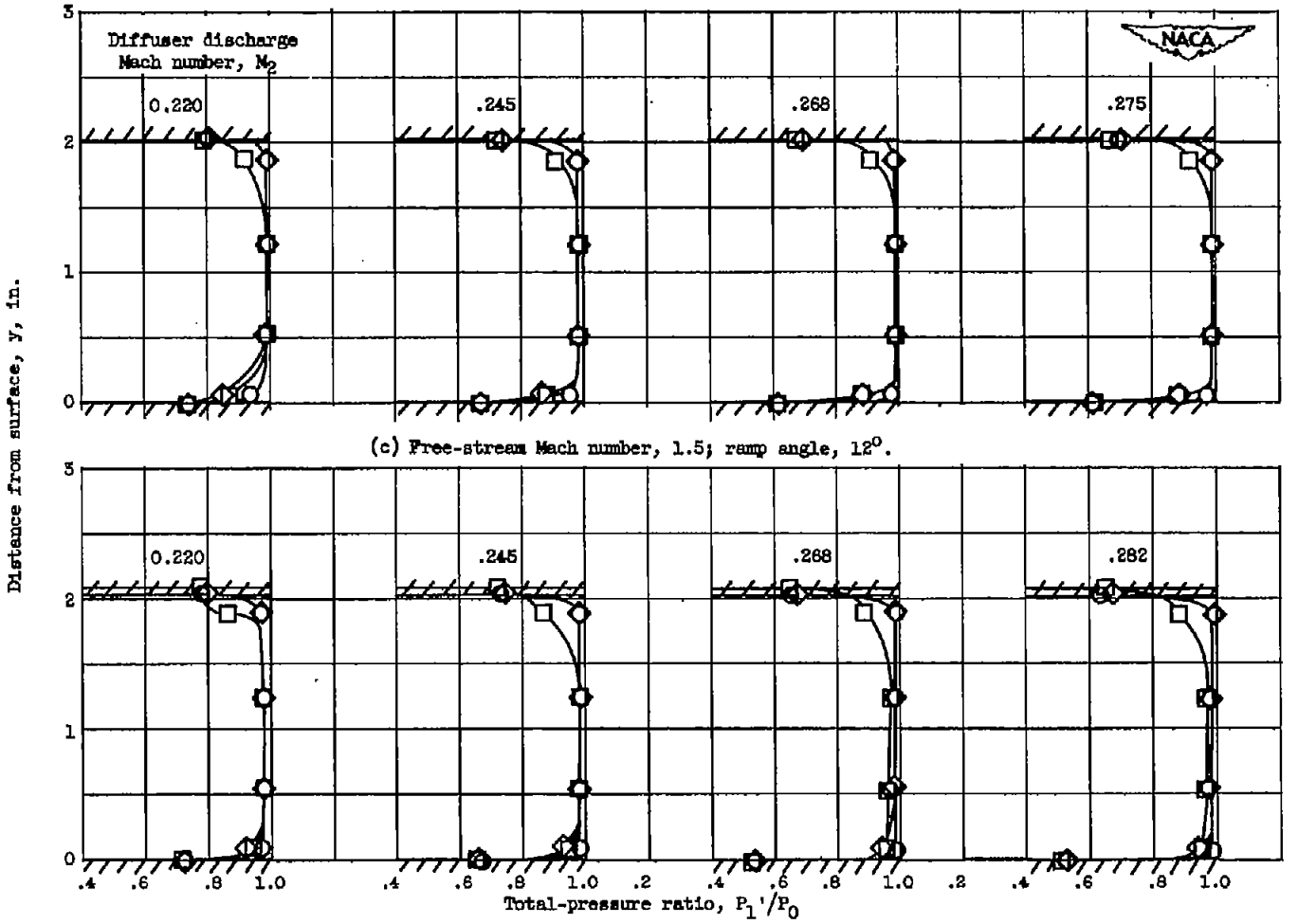

(c) Free-stream Mach number, 1.5; ramp angle, 12°.

(d) Free-stream Mach number, 1.5; ramp angle, 12°; side fairings.

Figure 8. - Continued. Inlet entrance total-pressure ratio profiles for inlets with 12° and 6° ramp angles with and without inlet side fairings at free-stream Mach numbers of 1.5 and 2.0 and angle of attack of 3°.

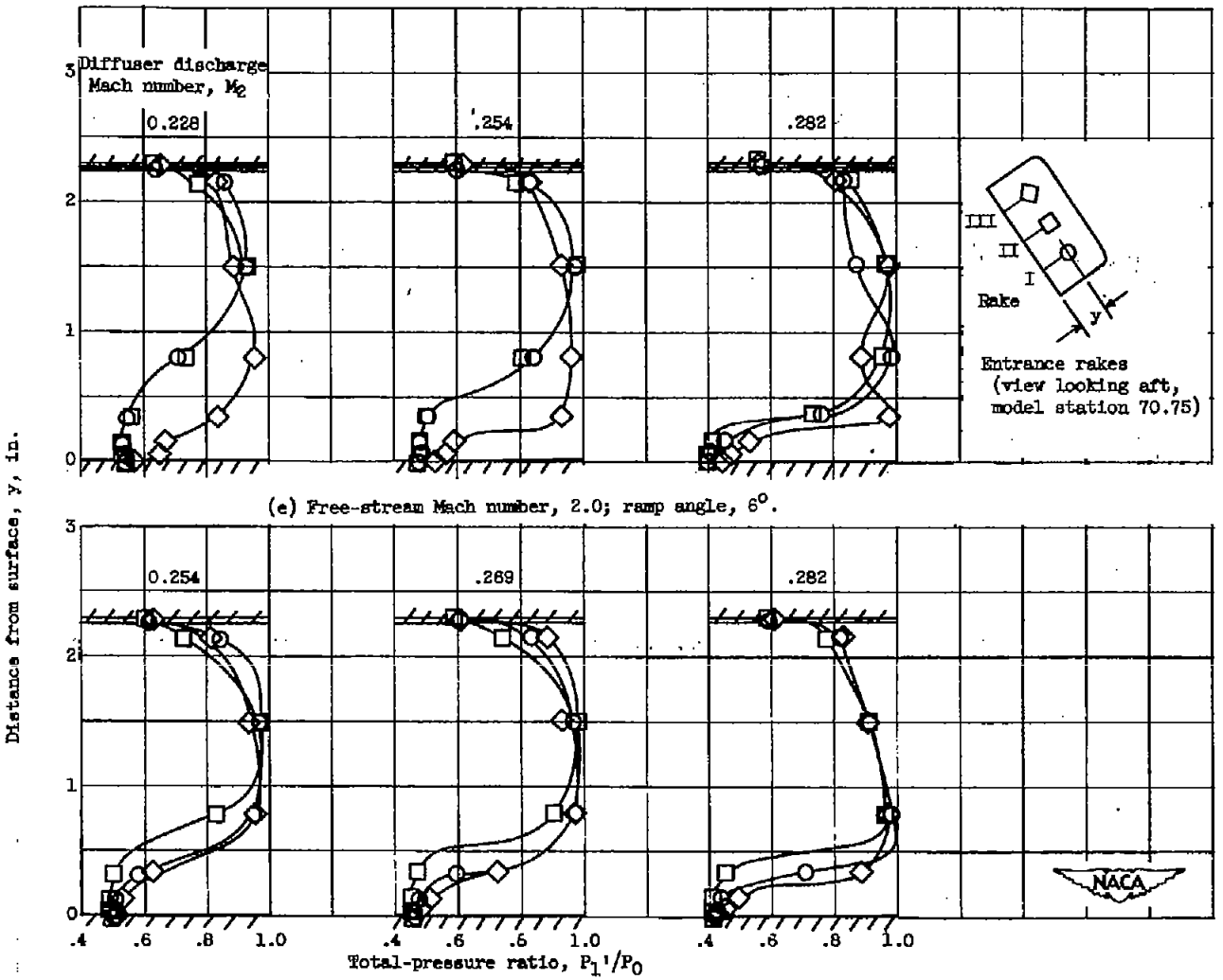

(e) Free-stream Mach number, 2.0; ramp angle, 6°.

(f) Free-stream Mach number, 2.0; ramp angle, 6°; side fairings.

Figure 8. - Concluded. Inlet entrance total-pressure ratio profiles for inlets with 12° and 6° ramp angles with and without inlet side fairings at free-stream Mach numbers of 1.5 and 2.0 and angle of attack of 3°.

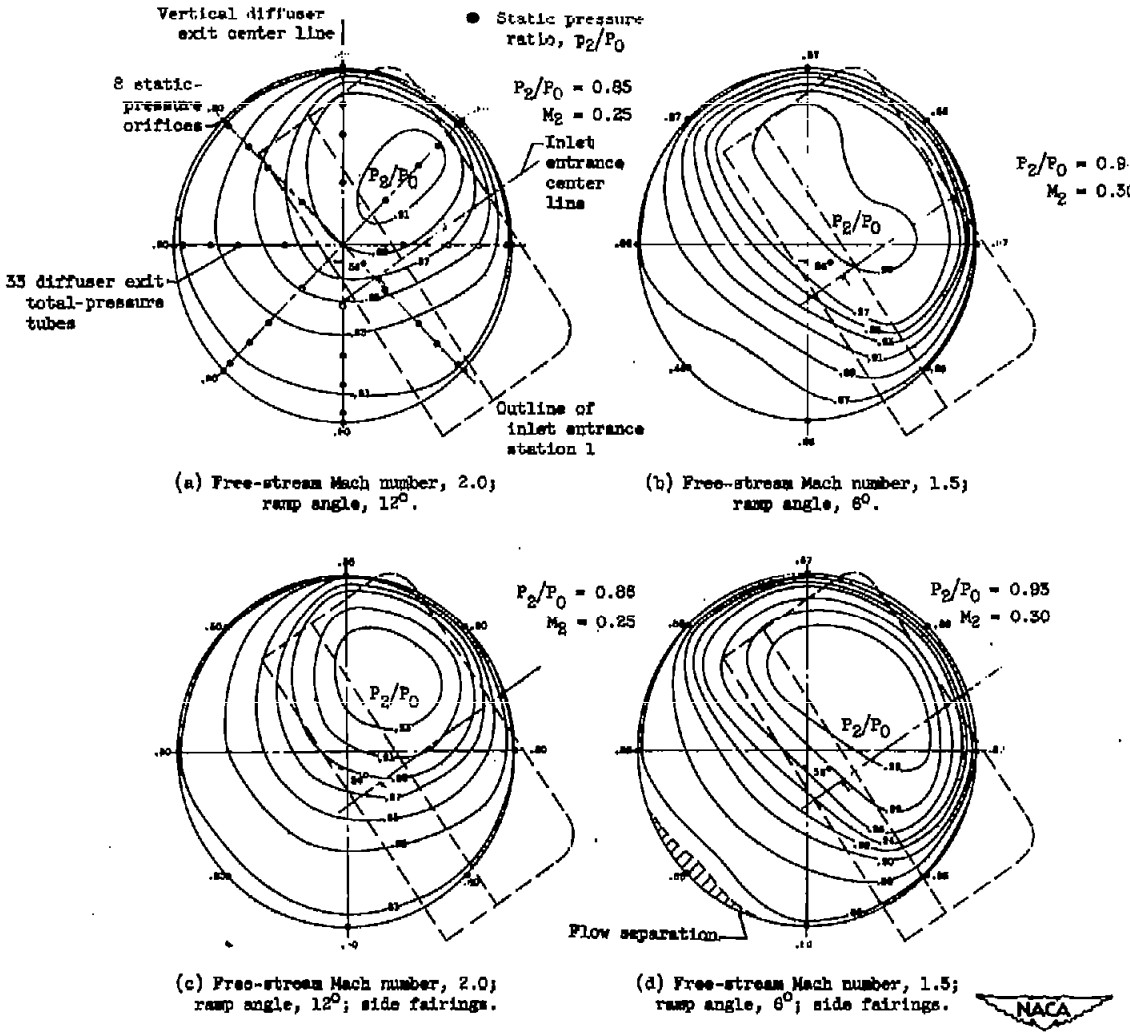

(a) Free-stream Mach number, 2.0; ramp angle, 12°.

(b) Free-stream Mach number, 1.5; ramp angle, 6°.

(c) Free-stream Mach number, 2.0; ramp angle, 12°; side fairings.

(d) Free-stream Mach number, 1.5; ramp angle, 6°; side fairings.

Figure 9. - Diffuser exit total-pressure contours for inlets with 12° and 6° ramp angles with and without inlet side fairings at free-stream Mach numbers of 2.0 and 1.5, respectively, and angle of attack of 5° at station 2 (view looking aft).

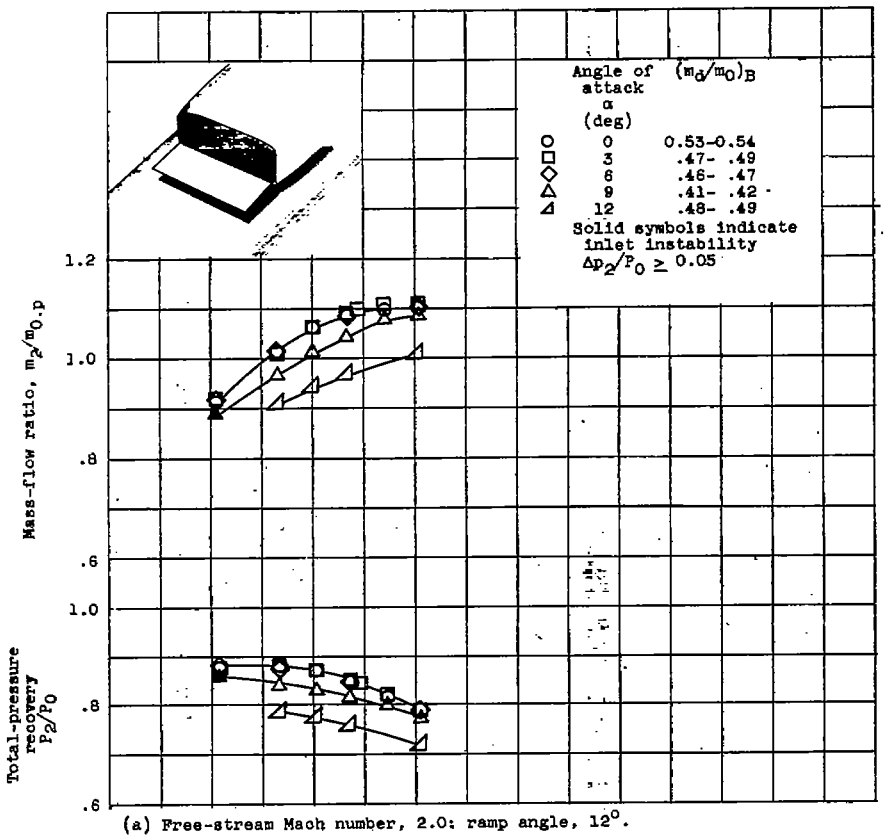

(a) Free-stream Mach number, 2.0; ramp angle, 12°.

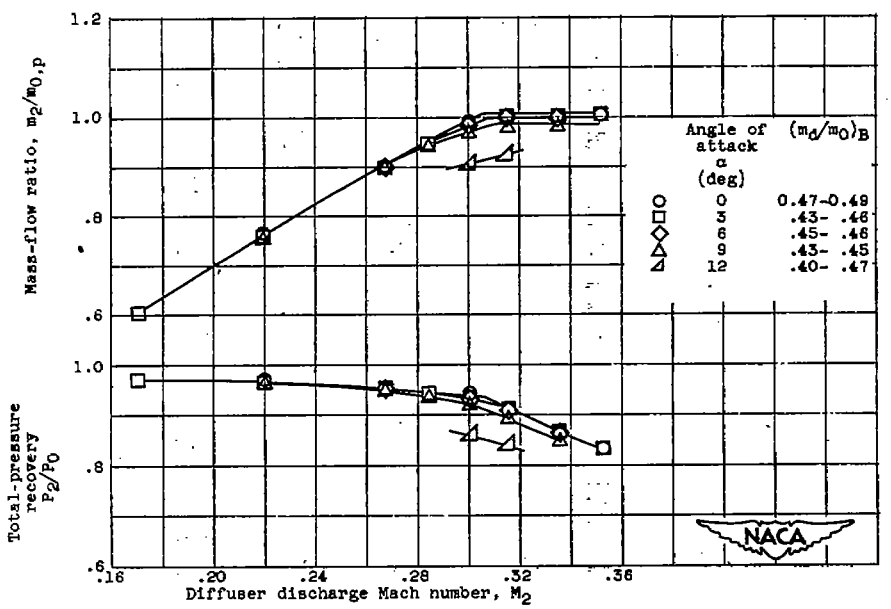

(b) Free-stream Mach number, 1.5; ramp angle, 6°.

Figure 10. - Variation of inlet flow characteristics with diffuser discharge Mach number at various supersonic flight Mach numbers, inlet ramp angles, and angles of attack.

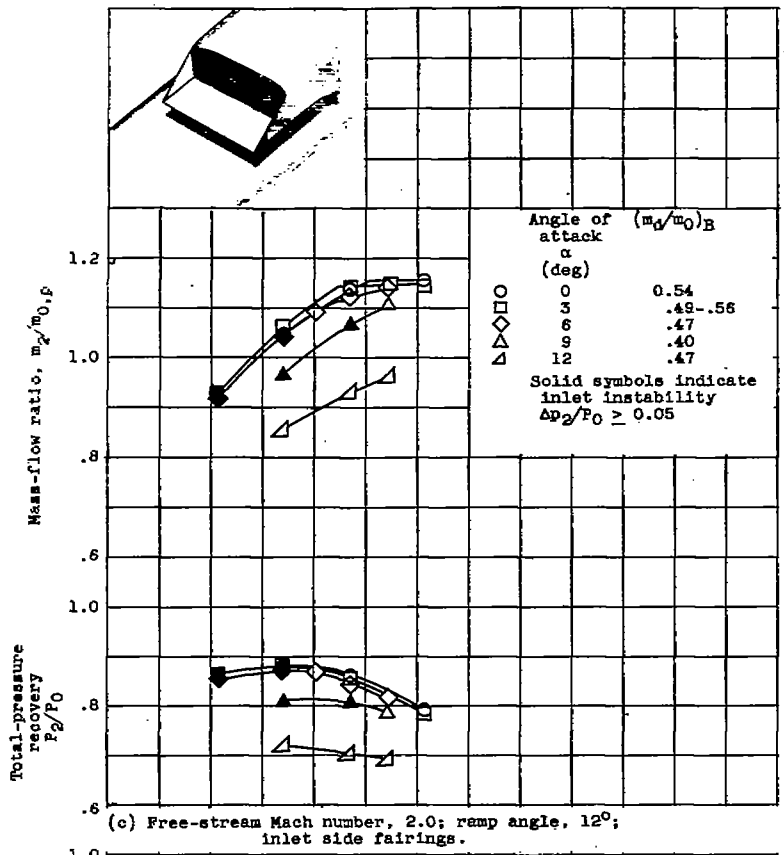

(c) Free-stream Mach number, 2.0; ramp angle, 12°; inlet side fairings.

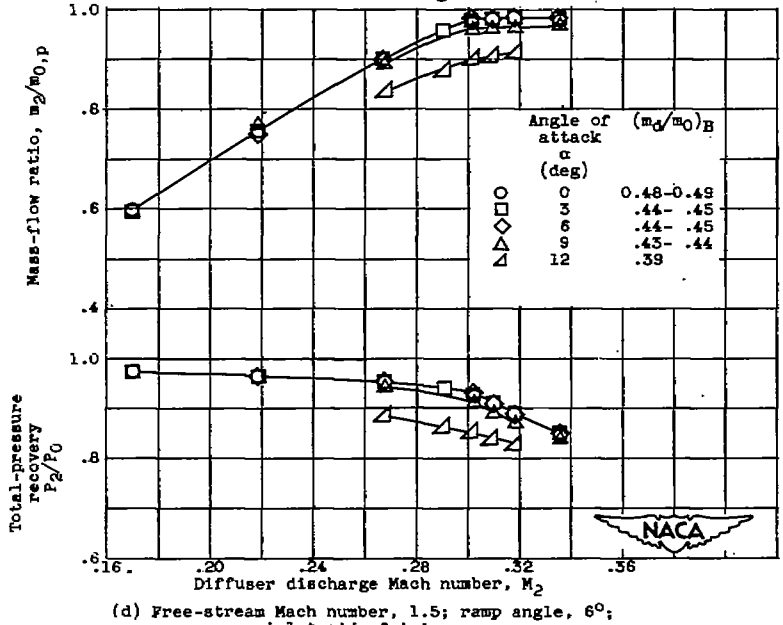

(d) Free-stream Mach number, 1.5; ramp angle, 6°; inlet side fairings.

Figure 10. - Concluded. Variation of inlet flow characteristics with diffuser discharge Mach number at various supersonic flight Mach numbers, inlet ramp angles, and angles of attack.

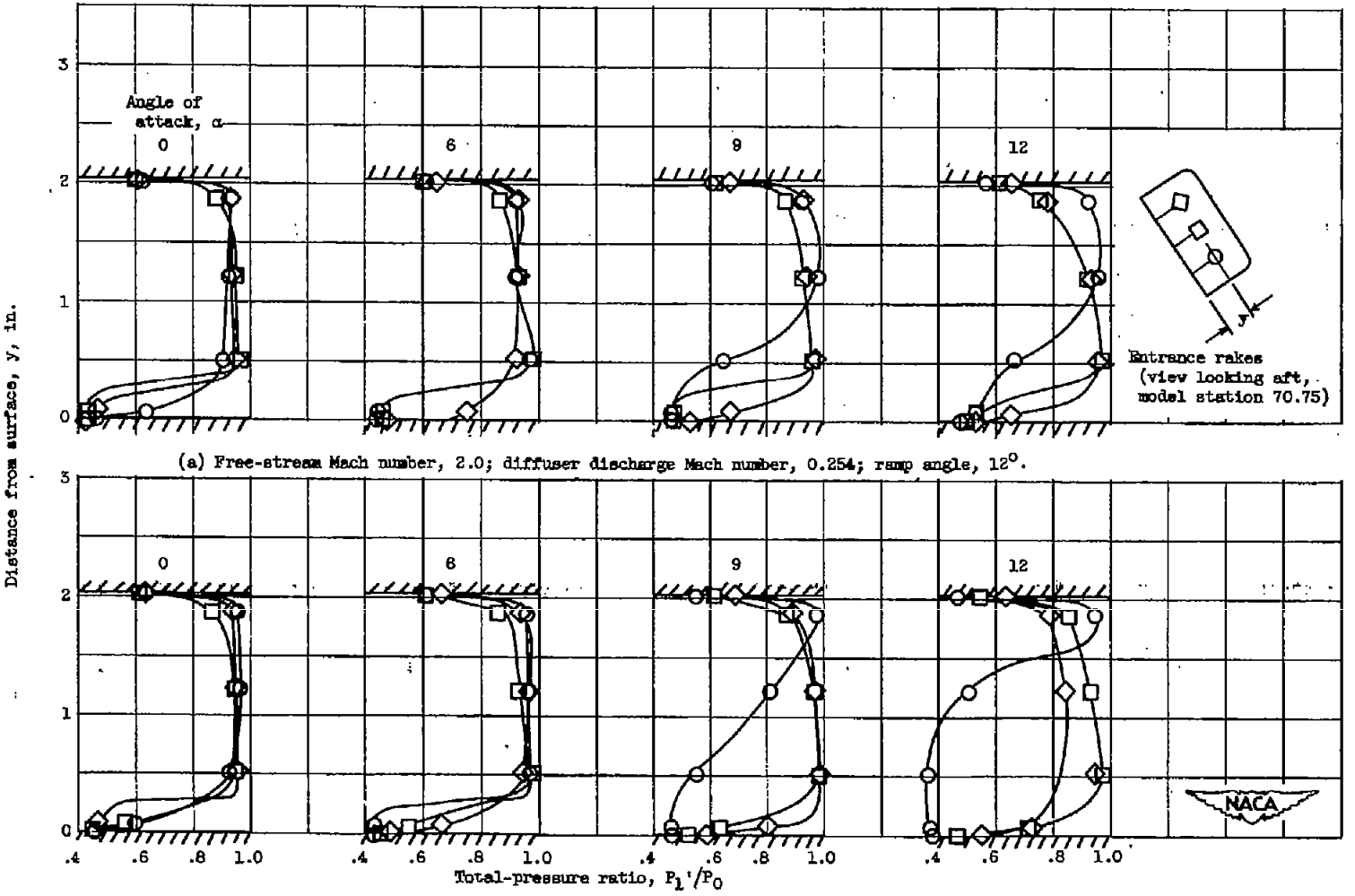

(a) Free-stream Mach number, 2.0; diffuser discharge Mach number, 0.254; ramp angle, 12°.

(b) Free-stream Mach number, 2.0; diffuser discharge Mach number, 0.254; ramp angle, 12°; side fairings.

Figure 11. - Inlet entrance total-pressure ratio profiles for inlets with 12° and 6° ramp angles with and without inlet side fairings at free-stream Mach numbers of 1.5 and 2.0 and various angles of attack.

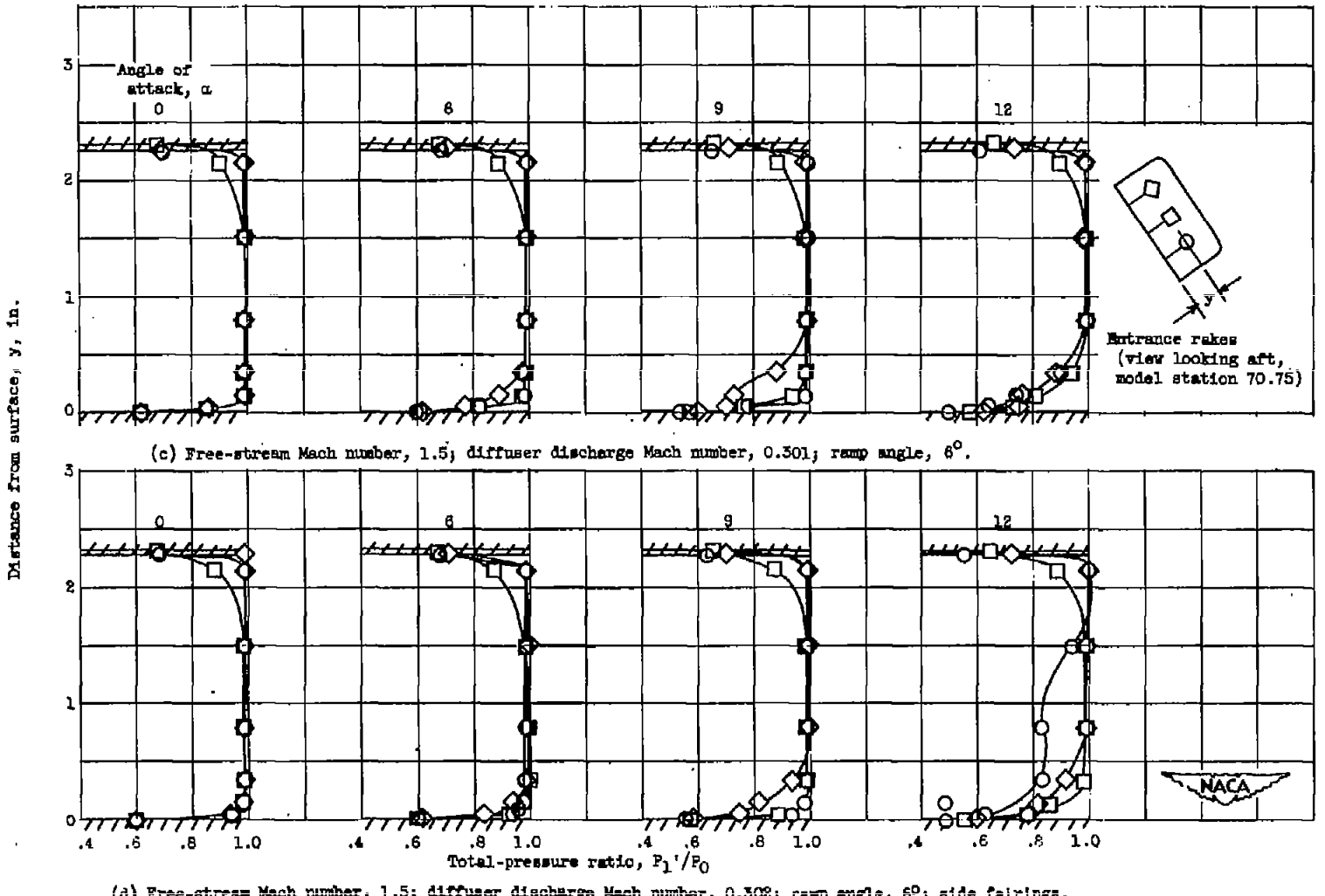

(c) Free-stream Mach number, 1.5; diffuser discharge Mach number, 0.301; ramp angle, 6°.

(d) Free-stream Mach number, 1.5; diffuser discharge Mach number, 0.302; ramp angle, 6°; side fairings.

Figure 11. - Concluded. Inlet entrance total-pressure ratio profiles for inlets with 12° and 6° ramp angles with and without inlet side fairings at free-stream Mach numbers of 1.5 and 2.0 and various angles of attack.

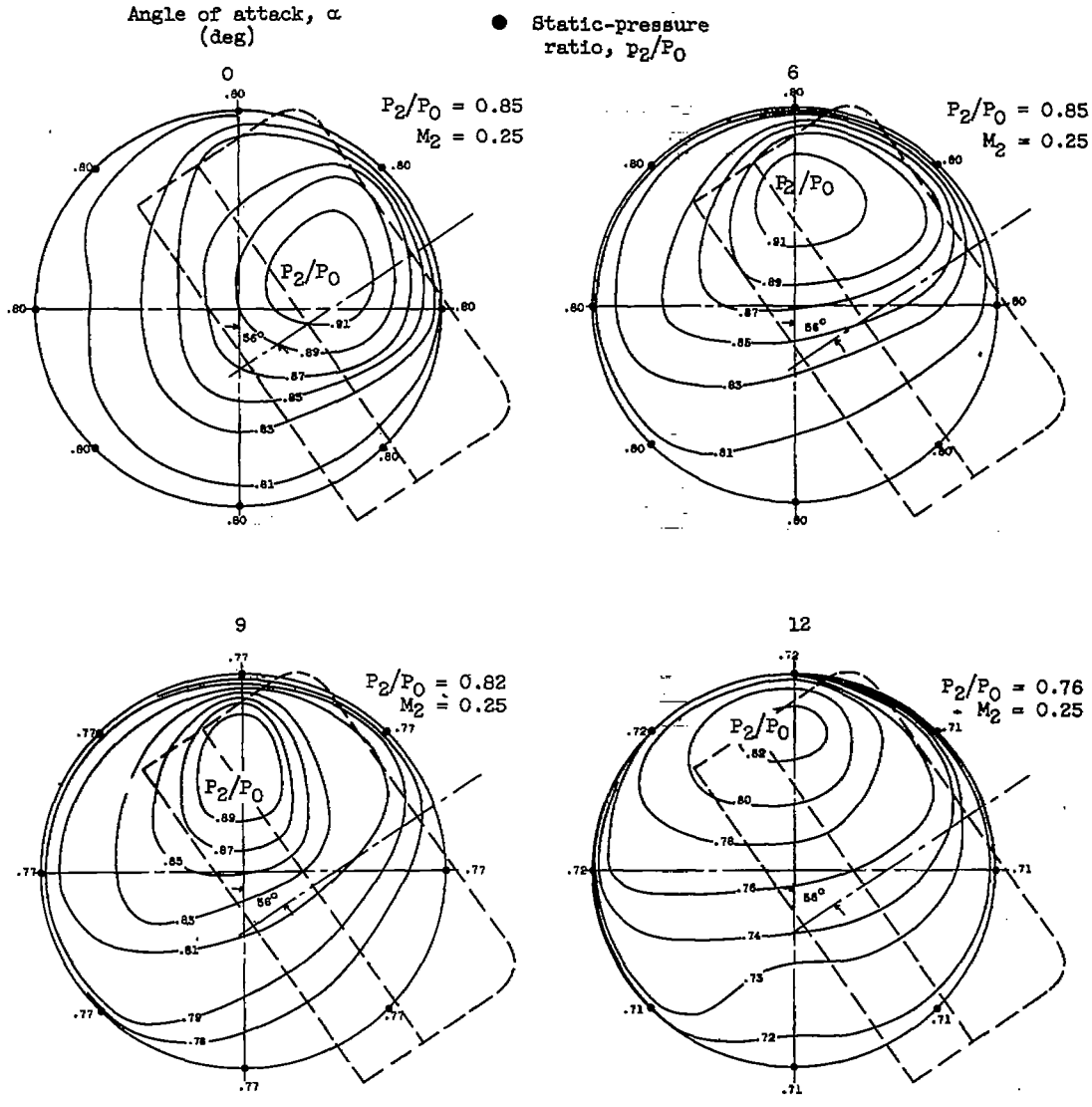

(a) Without inlet side fairings.

Figure 12. - Diffuser exit total-pressure contours for inlet operating at free-stream Mach number of 2.0, ramp angle of 12°, and various angles of attack at station 2 (view looking aft).

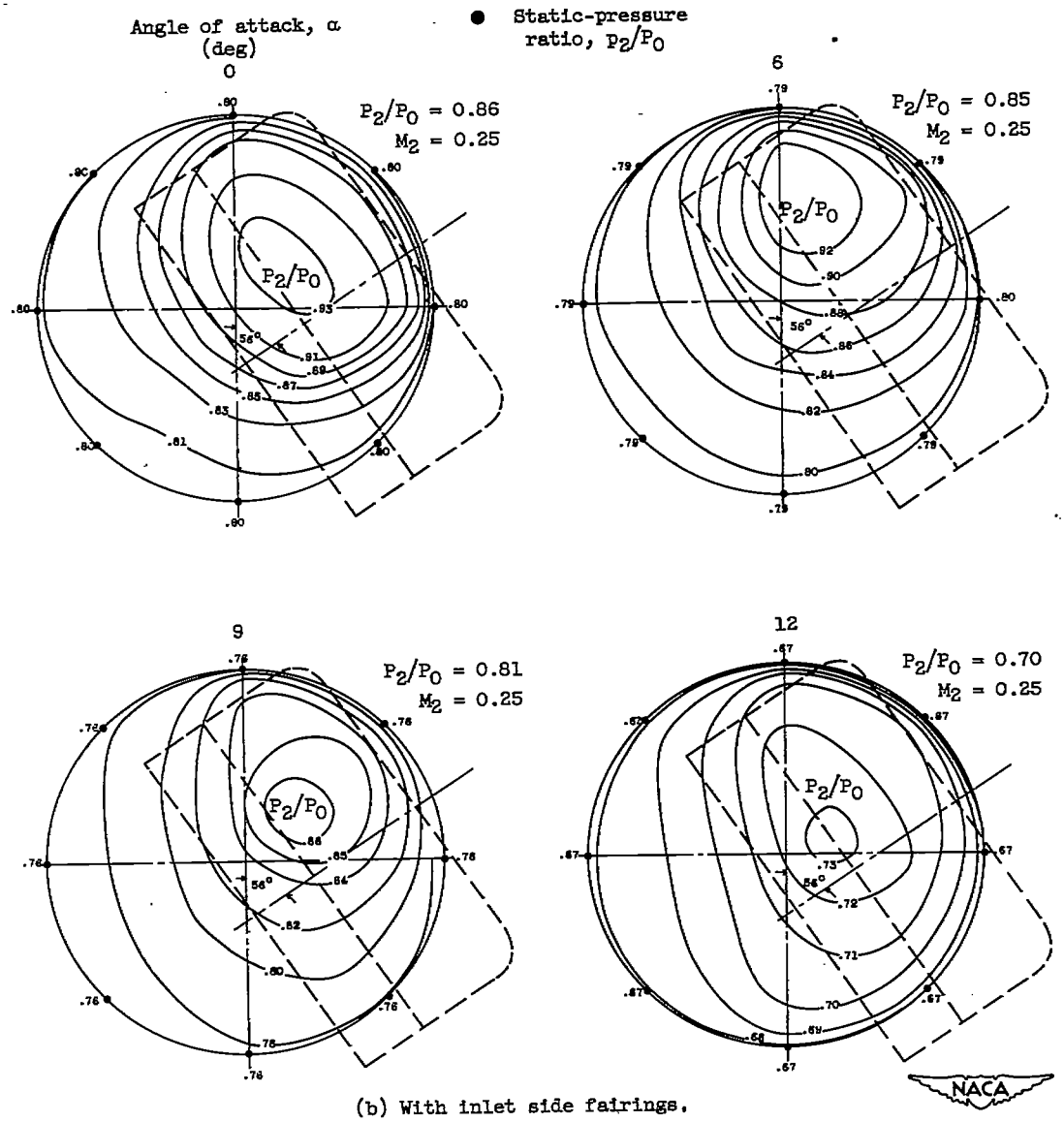

(b) With inlet side fairings.

Figure 12. - Concluded. Diffuser exit total-pressure contours for inlet operating at free-stream Mach number of 2.0, ramp angle of 12°, and various angles of attack at station 2 (view looking aft).

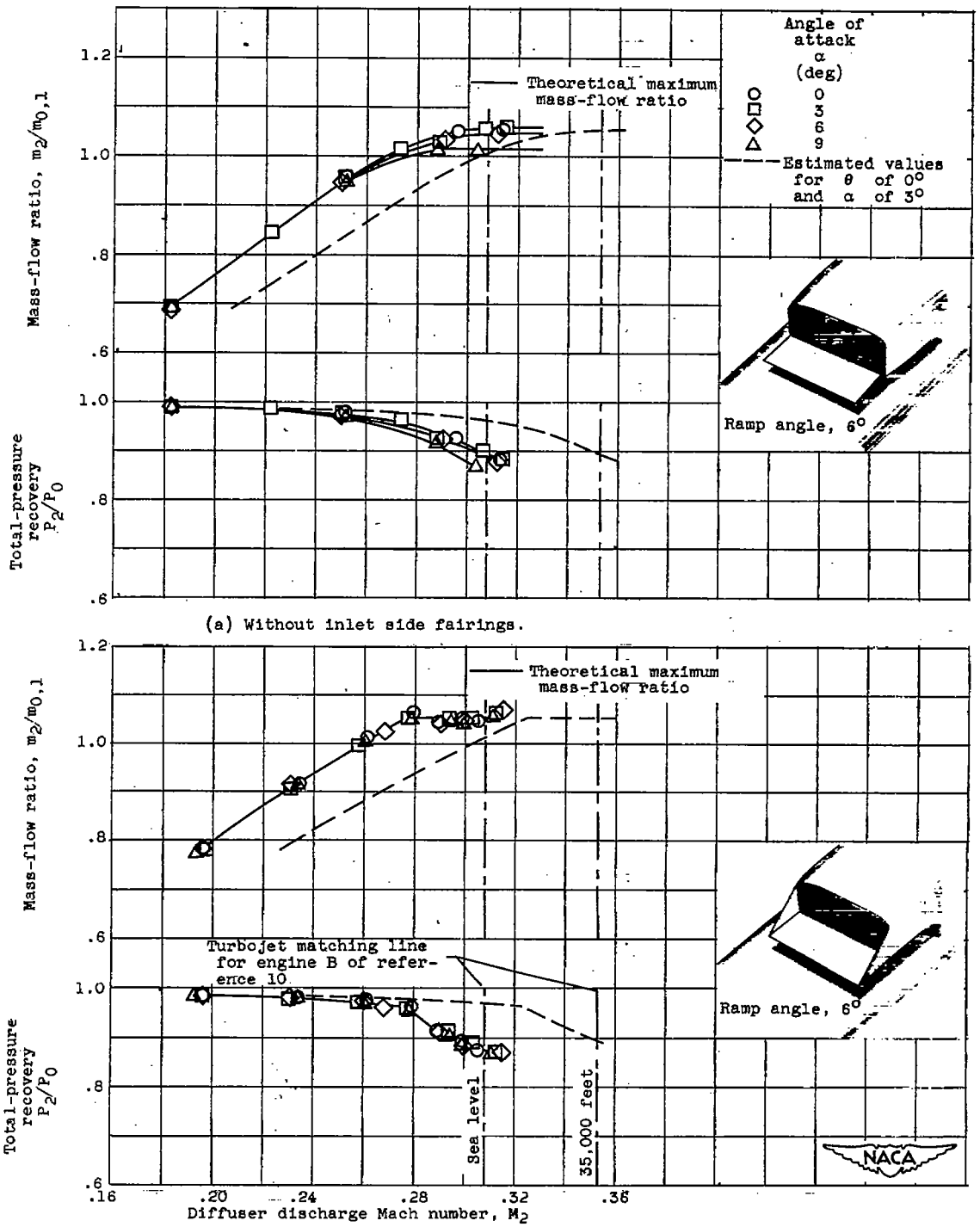

Figure 13. - Variation of inlet flow characteristics with diffuser discharge Mach number for inlets with 6° ramp angles with and without inlet side fairings at free-stream Mach number of 0.63 and various angles of attack.

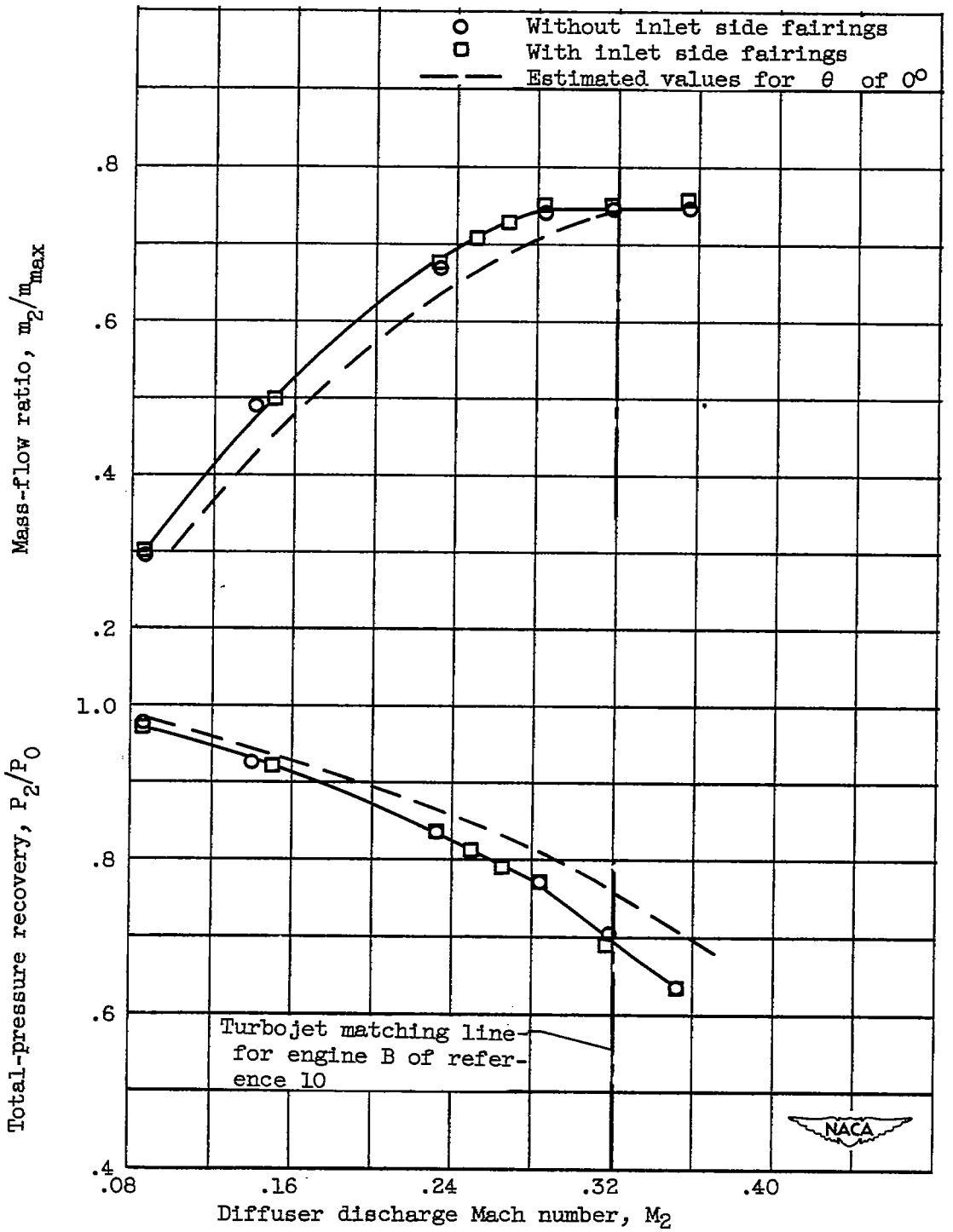

Figure 14. - Variation of inlet flow characteristics with diffuser discharge Mach number at static or take-off conditions for the 6° ramp rectangular inlets with and without inlet side fairings.

NACA-Langley - 10-28-52 - 400